Incompressible limit of a continuum model of tissue growth with segregation for two cell populations

Alina Chertock, Pierre Degond, Sophie Hecht, Jean-Paul Vincent

Mathematical Biosciences and Engineering

http://www.aimspress.com/journal/MBE

MBE, 16(5): 5804–5835
DOI: 10.3934/mbe.2019290
Received: 27 February 2019
Accepted: 17 June 2019
Published: 22 June 2019

Research article

Incompressible limit of a continuum model of tissue growth with segregation for two cell populations

Alina Chertock[1], **Pierre Degond**[2,*], **Sophie Hecht**[2,3] **and Jean-Paul Vincent**[3]

[1] Department of Mathematics, North Carolina State University, Raleigh, NC 27695, USA
[2] Department of Mathematics, Imperial College London, London SW7 2AZ, UK
[3] Francis Crick Institute, 1 Midland Rd, London NW1 1AT, UK

* **Correspondence:** Email: p.degond@imperial.ac.uk.

Abstract: This paper proposes a model for the growth of two interacting populations of cells that do not mix. The dynamics is driven by pressure and cohesion forces on the one hand and proliferation on the other hand. Contrasting with earlier works which assume that the two populations are initially segregated, our model can deal with initially mixed populations as it explicitly incorporates a repulsion force that enforces segregation. To balance segregation instabilities potentially triggered by the repulsion force, our model also incorporates a fourth order diffusion. In this paper, we study the influence of the model parameters thanks to one-dimensional simulations using a finite-volume method for a relaxation approximation of the fourth order diffusion. Then, following earlier works on the single population case, we provide formal arguments that the model approximates a free boundary Hele Shaw type model that we characterise using both analytical and numerical arguments.

Keywords: tissue growth; two cell populations; incompressible limit; free boundary problem

1. Introduction

During development, tissues and organs grow while generating diverse cell types. Thus, different cell populations co-exist during growth. For example, in a developing limb, prospective muscles, bone and epidermis become distinct during development and as a result grow at different rates. As they grow, these cell types contribute to mass gain for the whole structure. However, since the different cell populations grow at different rates, stresses arise and must be relieved to ensure that they contribute harmoniously to the final structure. How differential growth rates within a structure are accommodated is therefore an important question in developmental biology. To approach this question from a theoretical point of view, we consider a model whereby an idealised tissue is composed of one contiguous cell population located within a wider area occupied by another cell population.

Our approach relies on a new continuum model for two populations of cells which includes the following biological features. First, we impose a constraint that cells do not overlap. This is ensured in the model by an appropriate pressure-density relationship which becomes singular at the packing density. Second, we model cell-cell contact inhibition by implementing cell motion in the direction opposite to the cell density gradient. These features are believed to play important roles in the development of mono-layered epithelial tissues such as pseudo-stratified epithelia. Third, the model incorporates features that are specific to two non-mixing cell populations. The model favors segregation by penalizing the mixing of cells of different populations. Such segregation is observed in various tissues, such as developing tissues when there are two populations of cells which are genetically distinct, or cancerous tissues composed of proliferative and healthy cells. Some aspects of the derivation of our model use an optimal transport framework. Indeed, we describe the cell populations by means of continuum densities satisfying gradient flow equations which decrease a free energy encompassing some important biological properties of the system. Optimal transport has proved a fertile concept for many types of Partial Differential Equation (PDE) such as the porous medium equation [1], convection-diffusion equations [2], the Fokker Planck equation [3], etc. However, other aspects of the system such as the inclusion of reaction terms which model tissue growth depart from a strict optimal transport framework. So, optimal transport will not be used in this paper beyond the derivation of the model.

After describing the model, we first present numerical simulations in order to analyse the roles of the various parameters of the model. Then, we investigate its incompressible limit. In this limit, the cell densities can only take two values: either zero or their respective maximal value corresponding to the packing density. We show that the limit model is a free boundary Hele-Shaw model (HSM), which allows us to focus on the geometric evolution of the boundaries of the domains occupied by the two species.

Mathematical models have been widely used to study tissue development or tumour growth. Among these, we distinguish two ways of representing cells. On the one hand, discrete models consider each cell as an individual entity whose position and other attributes evolve in time [4, 5]. This provides a high level of accuracy but also results in large computational costs. On the other hand, continuum models consider local averages such as the cell number density, as functions of space and time, which evolve according to suitable PDEs [6, 7]. This description is appropriate when the number of cells is large as it dramatically reduces the computational cost. However it only gives access to the large scale features of the system as the small scale features are averaged out. As the goal of this paper is to study the evolution of the whole tissue, we have chosen a continuum model. Continuum models roughly fall into two categories. The first category comprises models which describe the dynamics of the cell density through convection and diffusion [8, 9, 10]. Models of the second category describe the motion of the geometric boundary between the tissue or the tumour and its environment through geometric evolution equations [11, 12, 13, 14]. The latter share similarities with Hele-Shaw models in fluid mechanics and Stefan's free boundary problem in solidification [15]. These two types of models are related to one another through asymptotic limits. In particular, some tumour growth models of the first type have been related to Hele-Shaw free boundary models in [16, 17, 18].

In this paper, we propose a two cell population model as an extension of earlier models for single cell populations introduced in [19, 16] in the context of tumour growth. In these works, the authors consider a single category of cells whose density is denoted by $n(x,t)$ and depends on time $t \geq 0$ and position $x \in \mathbb{R}^d$. The diffusion of the density is triggered by a mechanical pressure $p = p(n)$ which

is a given non linear function of the density n. Cell proliferation is modelled by a growth function $G = G(p)$ dependent on the pressure. The displacement of the cells occurs with a velocity $u = u(x,t)$ related to the pressure gradient through Darcy's law. The model is written as follows,

$$\partial_t n + \nabla \cdot (nu) = nG(p), \qquad \text{on } \mathbb{R}^+ \times \mathbb{R}^d, \tag{1.1}$$

$$u = -\nabla p, \qquad p = p(n). \tag{1.2}$$

In [16, 17, 18] the pressure is expressed as

$$p(n) = \frac{\gamma}{\gamma - 1} n^{\gamma - 1}, \tag{1.3}$$

where $\gamma > 0$ is a model parameter. Inserting (1.3) into (1.1), (1.2) leads to the porous medium equation which has been widely studied [20]. This model can be expressed as the gradient flow (for the Wasserstein metric) of the following energy,

$$\mathcal{E}(n) = \int_{R^d} P(n(x))\, dx, \tag{1.4}$$

where P is a primitive of p, i.e. $\frac{\partial P}{\partial n} = p$.

The incompressible limit of this model corresponds to $\gamma \to +\infty$. It has been shown in [21] that this incompressible limit is a Hele-Shaw free boundary model which, classically, is used to describe the pattern of tumor growth [12, 22]. In two dimensions, the classical Hele-Shaw problem models an incompressible viscous fluid squeezed between two parallel flat plates. As more fluid is injected, the region occupied by the fluid expands. It has been shown that the incompressible limits of many PDEs converge towards Hele-Shaw type models [23, 24, 25, 22, 26]. This incompressible limit and the corresponding Hele-Shaw model have been shown to be particularly relevant to tumor growth modelling [16, 17].

In this paper, we present a new Segregation Pressure Model (SPM) for two cells populations which is built upon the gradient flow framework presented above. We introduce a free energy $\mathcal{E}(n_1, n_2)$ that depends on the cell densities of each cell population n_1 and n_2. The free energy encompasses a term similar to (1.4) which depends on the total cell density $n = n_1 + n_2$ and models both cell contact inhibition and packing. In addition we introduce active repulsion between cells of different types in order to enforce the segregation property, the latter being expressed as $r = n_1 n_2 = 0$, i.e. the two cell densities cannot be simultaneously non-zero. As this term induces repulsion forces and triggers instabilities, we also include regularising terms depending on the gradients ∇n_1, ∇n_2 inside the expression of the free energy. We pursue two goals. The first one is the formal derivation of the incompressible limit model which takes the form of a two species Hele-Shaw Model (HSM). The second goal is to develop a numerical method for the SPM which enables us to illustrate the validity of the limit HSM.

The pressure law (1.3) previously used in the literature does not prevent cells from overlapping. Indeed, with this expression, the cell density can take a value greater than $n = 1$, where the value $n = 1$ is supposed to be the maximal allowed cell density, corresponding to complete packing. In this paper we rather use the expression (instead of (1.3))

$$p_\epsilon(n) = \epsilon \frac{n}{1 - n}, \tag{1.5}$$

where $\epsilon > 0$ is a modelling parameter which plays a similar role as the parameter $1/\gamma$ in (1.3). With this expression, the pressure has a singularity at $n = 1$ which prevents the density to take values greater than $n = 1$. Similar pressure laws have been used in [21]. The limit $\gamma \to \infty$ is now replaced by $\epsilon \to 0$.

Systems with multiple populations are studied in many different areas. In chemistry, reaction-diffusion systems are used to model reacting chemical substances [27]. In population dynamics, these model are generalised into cross-diffusion systems in which the movement of one species can be induced by the gradient of the population of another species. In biology, Keller-Segel models [28] are used to model bacterial chemotaxis. Another classical example of cross-diffusion in biology is the Lotka-Volterra model [29], which describes the dynamics of a predator-prey system. These have been extended to nonlinear diffusion Lotka-Volterra systems to model cell populations [30, 31]. In the context of tumor growth, systems with different types of cells have been studied (such as healthy/tumor cells, proliferative/quiescent cells [32, 33, 34]). Among these models [30, 31, 35], some preserve the segregation of initially segregated populations. On the other hand, some models generate segregation between initially non-segregated species. The ability of imposing segregation is a distinctive feature of the present work. The Cahn-Hilliard equation gives an example of a model that promotes segregation. It describes the process of phase separation [36] where, in the absence of growth terms and up to possible boundary effects, each phase tends to occupy a single connected domain from which it excludes the other phase. Similarities between our model and the Cahn-Hilliard equation will be described below.

The paper is divided into the following five sections. In Section 2 the two populations SPM model is described and numerical simulations which study the influence of the modelling parameters are shown. In Section 3, the main results are exposed: the formal incompressible limit theorem is stated; a formal proof of the convergence to the HSM free boundary problem is given; numerical simulations are shown in support and a discussion is provided. Then, Section 4 contains the description of the numerical scheme. A short conclusion is given in Section 5. Finally, Appendix A is devoted to the the derivation of the model from the free energy.

2. The Segregation Pressure model

2.1. Introduction of the continuum model

In this paper, we consider two densities of cells denoted by $n_1(t, x)$ and $n_2(t, x)$ and the corresponding pressures $p_1(t, x)$ and $p_2(t, x)$ that depend on time $t \geq 0$ and position $x \in \mathbb{R}^d$. We derive our model from the single cell model exposed in the introduction and define the free energy $\mathcal{E}(n_1, n_2)$ expressed as follows:

$$\mathcal{E}(n_1, n_2) = \int_{\mathbb{R}^d} P_\epsilon(n_1 + n_2)dx + \int_{\mathbb{R}^d} Q_m(n_1 n_2)dx + \frac{\alpha}{2}\int_{\mathbb{R}^d} (|\nabla n_1|^2 + |\nabla n_2|^2)dx, \tag{2.1}$$

where $\alpha > 0$ is a diffusion parameter and $\epsilon > 0$, $m > 0$ are parameters which set the strengths of the congestion and segregation effects in the pressure laws. The functions P_ϵ and Q_m are primitives of the functions p_ϵ and q_m defined respectively by (1.5) and

$$q_m(r) = \frac{m}{m-1}((1 + r)^{m-1} - 1). \tag{2.2}$$

From now, the total density will be denoted by $n = n_1 + n_2$ and the product of the densities will be denoted by $r = n_1 n_2$. The first term corresponds to the pressure building up from the volume exclusion

constraint and the second term is a repulsion pressure between the two different categories of cells. The last term represents cohesive energy penalising strong gradients of either cell densities. The effect of these different terms are detailed below.

For the sake of simplicity, we omit the parameters ϵ, m, α in the notations of the unknown functions n_1, n_2, p_1 and p_2. From the free energy (2.1), in Section A, we derive the following system of equations,

$$\partial_t n_1 - \nabla_x(n_1 \nabla p_1) + \alpha \nabla_x(n_1 \nabla(\Delta n_1)) = n_1 G_1(p_1), \tag{2.3}$$

$$\partial_t n_2 - \nabla_x(n_2 \nabla p_2) + \alpha \nabla_x(n_2 \nabla(\Delta n_2)) = n_2 G_2(p_2), \tag{2.4}$$

$$p_1 = p_\epsilon(n_1 + n_2) + n_2 q_m(n_1 n_2), \tag{2.5}$$

$$p_2 = p_\epsilon(n_1 + n_2) + n_1 q_m(n_1 n_2), \tag{2.6}$$

where G_1 and G_2 are growth functions depending of the pressures p_1 and p_2. The pressures p_1 and p_2 are obtain thanks to the formula

$$p_i = \partial_{n_i}[P_\epsilon(n_1 + n_2) + Q_m(n_1 n_2)] \text{ for } i = 1, 2.$$

We first comment on the first term of (2.1). We assume that the two categories of cells have identical volume, so that the volume exclusion pressure resulting from either category of cells is similar and the total volume exclusion pressure is just a function of the total cell density. The parameter ϵ is supposed to be small. So, this first term penalizes configurations where the total density n is close to the packing density (here assumed to be equal to 1 according to (1.5)).

We now comment on the second term of (2.1). The segregation pressure is a novel aspect of the model. To minimise the second term of the free energy, it is necessary to make $n_1 n_2$ as small as possible. In the particular case $\alpha = 0$, for a given density $n = n_1 + n_2$, the minimiser of the free energy will be (n_1^*, n_2^*) such that $n_1^* n_2^* = 0$ and $n = n_1^* + n_2^*$. This justifies why the repulsion term tends to increase the segregation of the populations as time evolves. Moreover this term imposes segregation when m is going to infinity. This can be seen thanks to the equality $(1 + r)(\frac{m-1}{m} q_m(r) + 1) = (\frac{m-1}{m} q_m(r) + 1)^{\frac{m}{m-1}}$. Passing to the limit $m \to \infty$, we obtain

$$(1 + r^\infty)(q^\infty + 1) = \lim_{m \to +\infty} (1 + r)(\frac{m-1}{m} q_m(r) + 1) = \lim_{m \to +\infty} (\frac{m-1}{m} q_m(r) + 1)^{\frac{m}{m-1}} = q^\infty + 1,$$

meaning that $r^\infty(q^\infty + 1) = 0$. Since $q^\infty \geq 0$, this implies that $r^\infty = 0$, which expresses the segregation property (the cell densities cannot be simultaneously non-zero).

The third term of the free energy is a cohesive energy. Indeed this term penalises the gradients of either densities, meaning that it tends to regroup each species in a single cluster. This term also allows the two populations to mix over a small width at their interface. The diffusion coefficient α is related to the width of the mixing region. To understand it, we make a rough order-of-magnitude calculation. We assume that the densities vary linearly in the mixing region supposed to occupy the region $[0, \ell]$. The density n_1 varies from a value close to 1 to the value 0 and n_2 varies in the opposite way, so: $n_1 \approx (1 - \nu)(1 - \frac{x}{l})$ and $n_2 \approx (1 - \nu)\frac{x}{l}$ with $\nu \ll 1$. We suppose that at the minimum of the free energy (2.1), the two last terms have the same order of magnitude in the interface zone. The first term of the free energy has been already taken into account by assuming that $n = n_1 + n_2 = 1 - \nu < 1$. We have,

$$Q(r) = \frac{1}{m-1}\Big((1 + r)^m - mr\Big) \approx \frac{1}{m-1}\Big((1 + (1 - \frac{x}{l})\frac{x}{l})^m - m(1 - \frac{x}{l})\frac{x}{l}\Big).$$

So by integrating on $[0, \ell]$ we get by a change of variables $z = (1-y)y$:

$$\begin{aligned}\int_0^\ell Q(r) &= 2\int_0^{\frac{1}{2}} \frac{1}{m-1}\Big((1+(1-y)y)^m - m(1-y)y\Big)dy \\ &= 2\int_0^{\frac{1}{4}} \frac{1}{m-1}\Big((1+z)^m - mz\Big)\frac{dz}{\sqrt{1-4z}} \\ &= C(m).\end{aligned}$$

When $m \gg 1$, the leading order term is $\frac{2}{m-1}\int_0^{\frac{1}{4}}(1+z)^m \frac{dz}{\sqrt{1-4z}}$ that we can estimate by neglecting $\frac{1}{\sqrt{1-4z}}$. We then get

$$C(m) \propto \lambda^m \tag{2.7}$$

where λ is a given constant. The fourth order term can be estimated by

$$\frac{\alpha}{2}\int_0^\ell |\nabla n_1|^2 + |\nabla n_2|^2 \approx \alpha\frac{(1-\nu)^2}{\ell^2}\ell \propto \frac{\alpha}{\ell}$$

We deduce that

$$\ell \propto \frac{\alpha}{C(m)} \propto \frac{\alpha}{\lambda^m}$$

At this stage it is interesting to see the analogy between our model and the Cahn-Hilliard equation. We recall that the Cahn-Hilliard equation is a gradient flow (for the L^2 distance) of the free energy

$$\mathcal{E}_{CH}(d) = \int (\frac{1}{4}(d^2-1)^2 + \frac{\gamma}{2}|\nabla d|^2)\, dx, \tag{2.8}$$

where $d = d(x)$ is the unknown function and $\gamma > 0$ is a modelling coefficient. In order to see the similarity with our model, we rewrite (2.1) in terms of the total density n and the difference $d = n_1 - n_2$ and let $m = 2$,

$$\begin{aligned}\mathcal{E}(n,d) =& \int P_\epsilon(n)dx + \int Q_2(\frac{n^2-d^2}{4})dx + \frac{\alpha}{8}\int (|\nabla(n+d)|^2 + |\nabla(n-d)|^2)dx \\ =& \frac{1}{16}\int (d^2-n^2)^2 dx + \frac{\alpha}{4}\int |\nabla d|^2 dx + \tilde{\mathcal{E}}(n),\end{aligned} \tag{2.9}$$

with $\tilde{\mathcal{E}}(n) = \int(1+P_\epsilon)dx + \frac{\alpha}{4}\int|\nabla n|^2 dx$. Now, fixing n and considering d as the only variable, we can ignore the term $\tilde{\mathcal{E}}(n)$. Then, the similarity of the first two terms of $\mathcal{E}(n,d)$ in (2.9) with (2.8) becomes clear. The only difference is that the two stable states $u = \pm 1$ of the Cahn-Hilliard energy are replaced by the states $d = \pm n$, which depend on n. Hence, we can view our model as a coupling between the Cahn-Hilliard equation for d, with a non linear parabolic equation for n. If we make $\alpha = 0$ in (2.1) and write the resulting equations in the unknowns (n, d), we obtain an unstable diffusion system, the repulsion pressure giving rise to negative diffusion. The role of the terms in factor of α in (2.1) is to counteract this instability by introducing a stable fourth order diffusion.

Note that the particular case $q_m = 0$ and $\alpha = 0$ has been studied in [30, 31, 35]. There, it has been shown that the system exhibits species segregation, provided that the initial conditions are segregated [32, 33, 37, 38]. The present paper treats a different case, as initially the two species may be mixed and

the model drives them to a segregated state after some time, except for a thin interface depending on α and m. This is consistent with the biological observation that some mixing between the cell species occurs across the interface.

The aim of this paper is to investigate the incompressible limit of this model (2.3)-(2.6), which consists of letting ϵ going to 0 and m going to infinity in the system.

2.2. Numerical simulations

In this section we present numerical simulation for both segregated and mixed initial populations. This section aims to illustrate the dynamics of the system and the role of the parameters ϵ, m, α in the volume exclusion pressure, the segregation pressure and the cohesive term. In order to facilitate the visualisation of the results, the simulation are performed in one dimension. The scheme used is described in Section 4.

2.2.1. Numerical simulation with initially segregated and mixed populations

We illustrate the evolution in time of the SPM on two initial configurations. For the first example, we consider initial densities which are segregated and distant, given by

$$n_1^{\text{ini}}(x) = 0.5e^{-5(x+0.5)^2} \quad \text{and} \quad n_2^{\text{ini}}(x) = 0.5e^{-5(x+1.5)^2}. \tag{2.10}$$

In the second example, the initial densities are mixed and given by

$$n_1^{\text{ini}}(x) = 0.7e^{-5x^2} \quad \text{and} \quad n_2^{\text{ini}}(x) = 0.5e^{-5(x-0.5)^2} + 0.6e^{-5(x+1)^2}. \tag{2.11}$$

With these two examples, we investigate cases where the initial densities are either segregated or mixed. For both examples, the growth functions are given by

$$G_1(p) = (20 - p) \quad \text{and} \quad G_2(p) = (10 - p), \tag{2.12}$$

and the numerical parameters are $\epsilon = 0.01$, $m = 10$, $\alpha = 0.01$. The numerical simulation of the SPM model will involve the use of an approximate model, the Relaxation Segregation Pressure Model (RSPM), detailed in Section 4. This relaxation model is introduced to facilitate the numerical treatment of the fourth order term in the SPM. The RSPM model involves a relaxation parameter ν which is given the value $\nu = 0.001$. The results of the simulations of Examples 1 and 2 are respectively plotted in Figure 1 and Figure 2. On these Figures, the red line represents the species n_1 and the blue line, the species n_2 on panels (a)-(d) while the orange and green lines respectively represent the pressures p and q on panels (e)-(h). For both figures, the initial densities and pressures are plotted on panel (a) and (e).

In Figure 1 (a)-(b), we observe the dynamics of the two populations when they are not yet in contact with each other. The dynamics is then similar to that of the one species model (1.1)-(1.2) (since the density of one species is equal to zero on the support of the other species). When the densities are smaller than 1, the pressure is small (cf Figure 1(e)) and the reaction terms control the dynamics, resulting in the growth of the densities. When the densities n_i reach the critical values $n_i^* = p^{-1}(p_i^*) = \frac{p_i^*}{\epsilon + p_i^*}$, with $p_1^* = 20$ and $p_2^* = 10$ (p_i^* is the value for which the growth functions vanish), the pressure p become significant and creates a moving front encompassing the domain where $n_i \approx n_i^*$ (cf Figure 1(c)-(d)). In panel Figure 1(c) the two populations meet, which creates an interface between

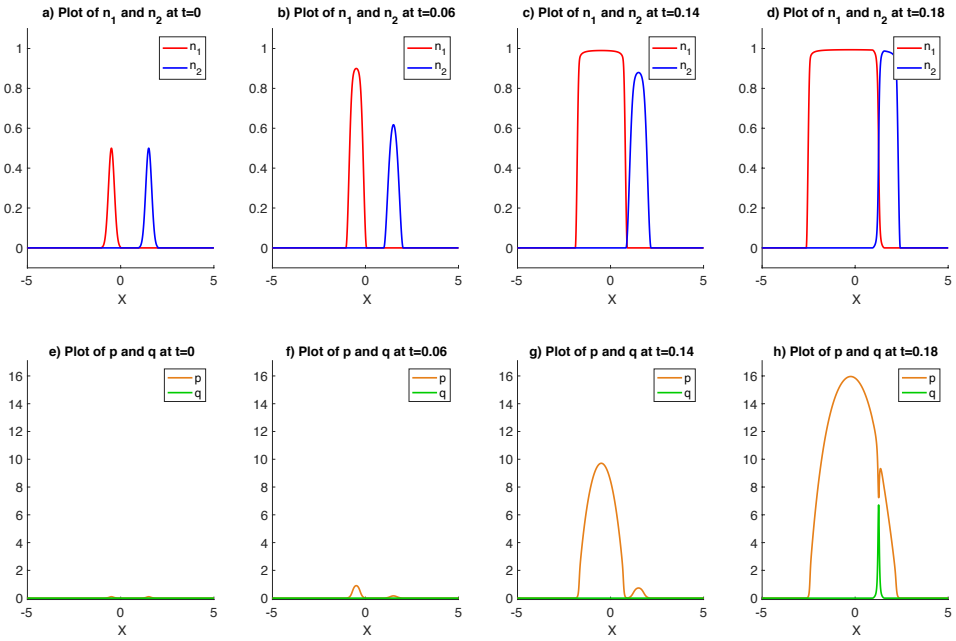

Figure 1. Densities n_1 (red), n_2 (blue) and pressures p (orange), q (green) as functions of position x for the SPM at different times: (a), (e) $t = 0$; (b), (f) $t = 0.06$; (c), (g) $t = 0.14$; (d), (h) $t = 0.18$. Initial conditions: densities from Eq. (2.10), growth function from Eq. (2.12).

them. In panel Figure 1(h), we observe a pressure ditch at the interface which is due to a small variation in the total density. This phenomenon will be investigated later when we will study the influence of the parameters m and α. Omitting the pressure ditch, we can consider that the gradient of the pressure is negative at the interface, which creates a movement of the interface toward the right. Indeed the red species, which has reached its critical density, is expanding and pushes the blue species to have more space to grow (cf Figure 1(d) and (h)).

In Figure 2, we observe the dynamics of two cell populations when they are initially mixed. When the overlapping between the two species is strong the dynamics is driven by the segregation pressure as q is nonnegative (cf Figure 2(i)). This creates domains where the density of one species is close to its maximal value while the other species density is close to 0. Because the parameter m which is the exponent of the segregation pressure is finite, some mixing is allowed between the two cell species. At the interfaces between the domains occupied by either species, we observe ditches in the pressure p, which are correlated with peaks in the segregation pressure q. In Figure 2(i-b)-(i-d), as the densities are close to their maximal value, the interfaces are moving in the directions given by the signs of the pressure gradients $\partial_x p$ (with p plotted in Figure 2(i-f)-(i-h)). In this case, the red species is growing faster than the blue one, which explains why the inner species is pushing the outer one to have more space to grow. In Figure 2 (ii), which corresponds to the same simulation as in Figure 2 (i) but for larger times, we observe on the left side that the red species pushes the blue species outside the domain, until only the red species remains (see Figure 2 (ii-d)). In addition, in Figure 2 (ii) we observe that a small pouch of the blue species surrounded by the red one gradually disappears. Because $20 = p_1^* > p_2^* = 10$, the pressure at the location of the blue species pouch becomes larger than $p_2^* = 10$ (as observed in Figure 2 (ii-e) and (ii-f)) and this triggers the decay of the blue population as its growth term becomes

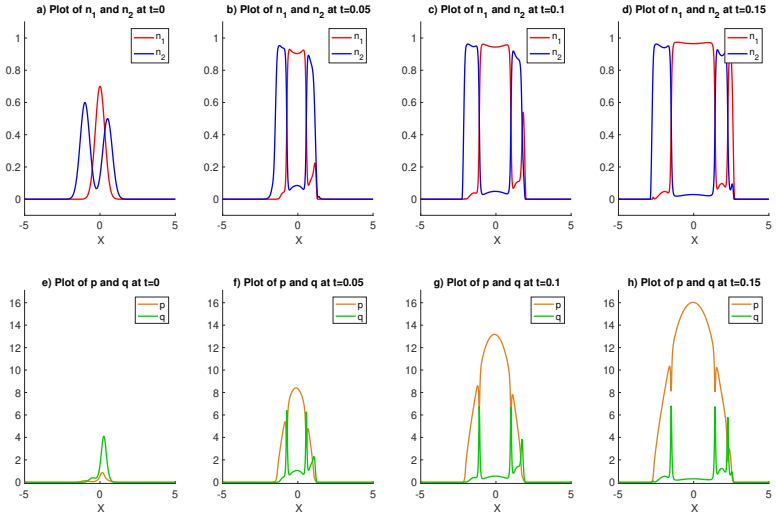

(a) Plot for small times: (a), (e) $t = 0$; (b), (f) $t = 0.05$; (c), (g) $t = 0.10$; (d), (h) $t = 0.15$

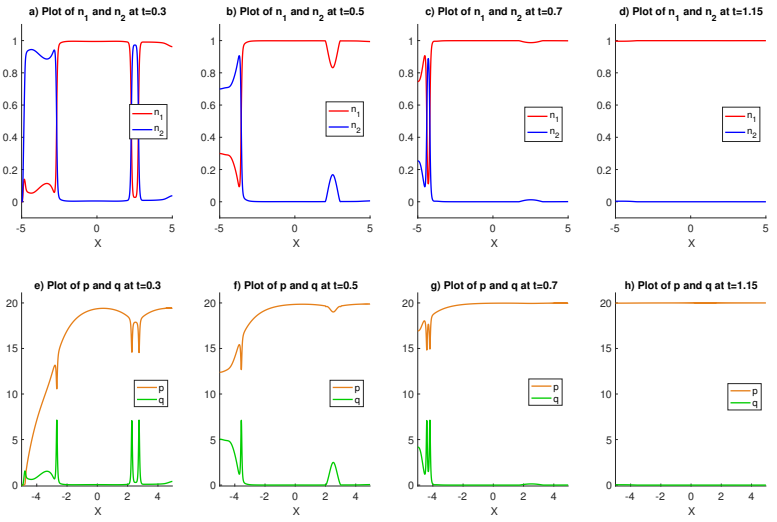

(b) Plot for large times: (a), (e) $t = 0.3$; (b), (f) $t = 0.5$; (c), (g) $t = 0.7$; (d), (h) $t = 1.2$

Figure 2. Densities n_1 (red), n_2 (blue) and pressures p (orange), q (green) as functions of position x for the SPM at small times (i) and large time (ii). Initial conditions: densities from Eq. (2.11), growth function from Eq. (2.12).

negative. At large times, only the faster growing species remains.

2.2.2. Influence of the parameters

In Figure 1 and Figure 2, we observe some mixing between the two populations: first, at the interface between their respective domains the species mix in a small interval and create a ditch in the pressure p; second, in the central domain occupied by the red species in Figure 2, the density of the blue species

is not exactly zero. To understand these phenomena we study the influence of the parameters ϵ, m, α and plot the simulation results respectively in Figure 3 (i), (ii), (iii) for a fixed time $t = 0.15$. The initial densities and growth functions are the same as in Example 2 of the previous subsection and are defined by Eqs. (2.11) -(2.12). We vary the parameters about pivot values given by $\epsilon = 0.01$, $m = 10$, $\alpha = 0.01$, $\nu = 0.001$.

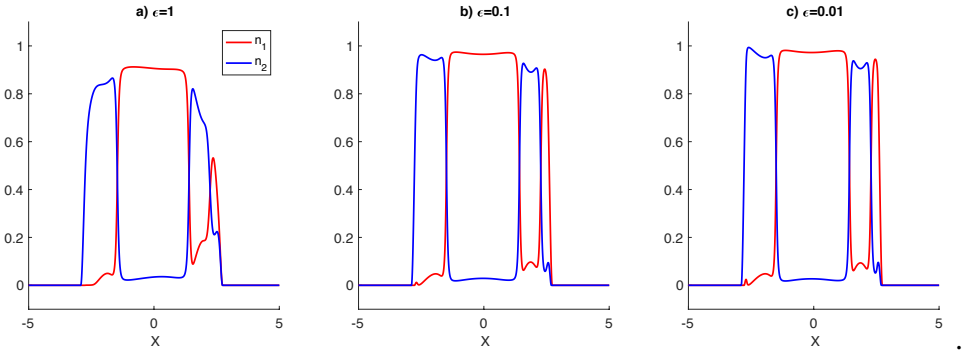

(a) Varying ϵ: $\epsilon = 1$ (a), $\epsilon = 0.1$ (b), $\epsilon = 0.01$ (c). The other parameters are $m = 10$, $\alpha = 0.01, \nu = 0.001$.

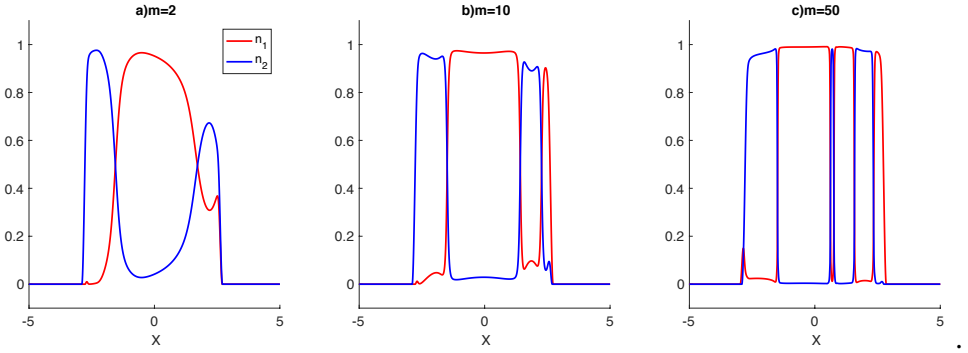

(b) Varying m: $m = 5$ (a), $m = 10$ (b), $m = 50$ (c). The other parameters are $\epsilon = 0.01$, $\alpha = 0.01, \nu = 0.001$.

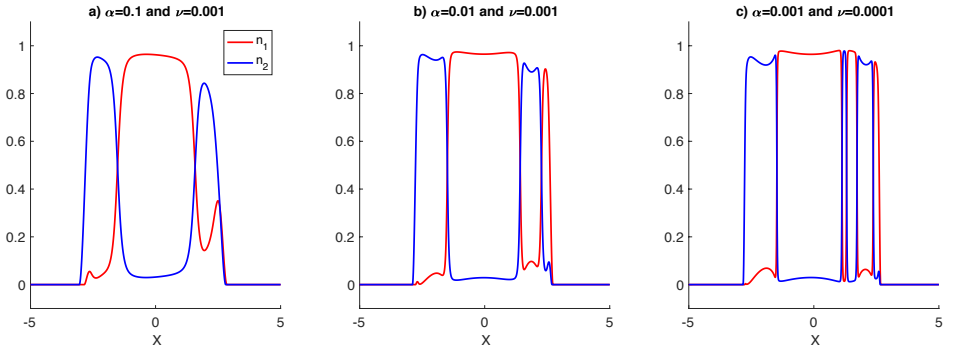

(c) Varying α and ν: $\alpha = 0.1, \nu = 0.001$ (a), $\alpha = 0.01, \nu = 0.001$ (b), $\alpha = 0.001, \nu = 0.0001$ (c). The other parameters are $\epsilon = 0.01$, $m = 10$.

Figure 3. Densities n_1 (red), n_2 (blue) as functions of position x for the SPM at time $t = 0.15$ for different values of the parameters ϵ (i), m (ii) and α (iii). Initial conditions: densities from Eq. (2.11), growth functions from Eq. (2.12).

In Figure 3 (i-a), (i-b), (i-c) the densities are plotted for the cases $\epsilon = 1$, $\epsilon = 0.1$ and $\epsilon = 0.01$ respectively. We first remark that the parameter ϵ does not influence the amount of mixing of the two populations or the number of domains each species is divided in. Instead ϵ influences the densities at the boundaries of the domains occupied by each species. As ϵ decreases, the gradients of the densities become sharper at the exterior boundaries and at the interfaces between the two populations. In addition, the upper bound of the densities increases and becomes closer to 1.

In Figure 3 (ii), the influence of the exponent of the segregation pressure m is studied. The densities are plotted for cases $m = 5$, $m = 10$ and $m = 50$ in Figure 3 (ii-a), (ii-b), (ii-c) respectively. In Figure 3(ii-c), we can observe that there is less mixing than in Figures 3(ii-a) and (ii-b). In Figure 3(ii-c) the central domain of the red species is smaller than in Figure 3(ii-b) because the blue species has grown in the middle as a result of a larger segregation pressure. Then in Figure 3(ii-c), we do not observe the small dimple in the blue cell density found in Figure 3(ii-a) and (ii-b). To summarise, the parameter m controls the strength of the segregation between the two populations. However, even when m is large, we still observe some mixing at the interfaces.

In Figure 3 (iii), we study the influence of the parameter α in factor of the fourth order diffusion term. The densities are plotted for the cases $\alpha = 0.1, \nu = 0.001$; $\alpha = 0.01, \nu = 0.001$ and $\alpha = 0.001, \nu = 0.0001$ in panels Figure 3 (iii-a), (iii-b), (iii-c) respectively (we have observed that the parameter ν needs to be smaller than α). We can observe that as α becomes smaller, the width of the interface region between the two populations gets smaller. We can also observe in Figure 3(iii-c) that on the right hand side, thin stripes with alternating populations appear. However, even when such stripes appear, there is still some mixing between the two populations, by contrast with the simulations where m was higher in Figure 3(ii-c). The same kind of features, namely the formation of many thin strips alternating $n_1 = 1$, $n_2 = 0$ and $n_1 = 0$, $n_2 = 1$, were observed in simulations performed with $\alpha = 0$. This was observed both with the same numerical scheme as that used in this paper, and with schemes using the gradient flow structure of the system. Without the fourth order term, a species surrounded by an other one will prefer to split, with some proportion of the population jumping across the other species instead of pushing it. For these reasons, the fourth order term is essential to produce realistic dynamics. What this analysis shows is that the choice of the parameter α is critical to prevent this jumping behaviour and maintain the connectivity of the domains occupied by the species.

3. Incompressible limit $\epsilon \to 0, m \to +\infty$ and $\alpha \to 0$

3.1. Formal limit

In this Section, we obtain formal convergence results of the model when $\epsilon \to 0$, $m \to \infty$ and $\alpha \to 0$. First we list some assumptions. As for the growth function, we assume:

$$\begin{cases} \exists\, G_m > 0, \quad \|G_1\|_\infty \le G_{\max}, \quad \|G_2\|_\infty \le G_{\max}, \\ G_1', G_2' < 0, \quad \text{and } \exists\, p_1^*, p_2^* > 0, \quad G_1(p_1^*) = 0 \text{ and } G_2(p_2^*) = 0, \\ \exists\, \gamma > 0, \quad \min(\min_{[0,p_1^*]} |G_1'|, \min_{[0,p_2^*]} |G_2'|) = \gamma. \end{cases} \tag{3.1}$$

These assumptions stem from biological considerations. As the pressure increases in the tissue, cell division occurs less frequently, until eventually the pressure reaches a critical value, which either stops the growth or starts to trigger cell death. In what follows, the growth functions will be chosen as

$G(p) = g(p^* - p)$. As for the initial conditions, we assume that there exists $\epsilon_0 > 0$ such that, for all $\epsilon \in (0, \epsilon_0)$,

$$\begin{cases} 0 \le n_1^{\text{ini}}, \quad 0 \le n_2^{\text{ini}}, \quad 0 \le n^{\text{ini}} := n_1^{\text{ini}} + n_2^{\text{ini}} \le 1, \\ p_\epsilon^{\text{ini}} := \epsilon \dfrac{n^{\text{ini}}}{1 - n^{\text{ini}}} \le p^* := \max(p_1^*, p_2^*). \end{cases} \tag{3.2}$$

Thanks to these assumptions, it is possible to establish a priori estimates on n_1 and n_2 such as positivity and L^1 bounds. However, in order to pass to the limits $\epsilon \to 0$, $m \to \infty$ and $\alpha \to 0$, we need more a priori estimates. In the following theorem, we only provide a formal limit. Indeed, the appearance of terms of the type $\nabla n \cdot \nabla r$ which we are not able to control prevent us from obtaining such theorem. The fourth order term is also difficult to control, as it does not enable us to use maximal principle arguments.

The main result is stated in the following theorem.

Theorem 1. *(Formal limit) Let $T > 0$, $Q_T = (0, T) \times \mathbb{R}^d$. Let G_1, G_2 and n^{ini}, n_1^{ini}, n_2^{sini} satisfy assumptions* (3.1) *and* (3.2)*. Suppose the limits of the densities $n_1(x, t)$, $n_2(x, t)$, of the pressure $p_\epsilon(x, t) = p_\epsilon(n_1(x, t), n_2(x, t))$ and of $q_m(x, t) = q_m(n_1(x, t), n_2(x, t))$ as $\epsilon \to 0$, $m \to +\infty$ and $\alpha \to 0$ exist and are denoted by n_1^∞, n_2^∞, p^∞ and q^∞. If the convergence is strong enough then these limits satisfy*

$$\partial_t n_1^\infty - \nabla \cdot (n_1^\infty \nabla p^\infty) = n_1^\infty G_1(p_1^\infty), \tag{3.3}$$

$$\partial_t n_2^\infty - \nabla \cdot (n_2^\infty \nabla p^\infty) = n_2^\infty G_2(p_2^\infty). \tag{3.4}$$

As a consequence of (3.3) *and* (3.4) *we have,*

$$\partial_t n^\infty - \Delta p^\infty = n_1^\infty G_1(p_1^\infty) + n_2^\infty G_2(p_2^\infty), \tag{3.5}$$

In addition, we have

$$(1 - n^\infty) p^\infty = 0, \tag{3.6}$$

with $n^\infty = n_1^\infty + n_2^\infty$,

$$n_1^\infty n_2^\infty = 0, \tag{3.7}$$

and the complementary relation

$$p^{\infty 2}(\Delta p^\infty + n_1^\infty G_1(p^\infty) + n_2^\infty G_2(p^\infty)) = 0. \tag{3.8}$$

Remark 1. The assumption $n_1^{\text{ini}} n_2^{\text{ini}} = 0$ is not needed in Theorem 1. Since in the limit, the segregation is imposed by (3.7), the system reorganises instantaneously and the initial density of the limit model must verify $n_1^{\infty\text{ini}} n_2^{\infty\text{ini}} = 0$. The densities $n_1^{\infty\text{ini}}$ and $n_2^{\infty\text{ini}}$ could be determined through an initial-layer analysis.

Firstly, it is important to notice that, in the limit, p^∞ and q^∞ become independent of the densities n_1^∞ and n_2^∞. Indeed, looking at the expression of the pressures (1.5)-(2.2) in the limit, we obtain:

$$p^\infty(n) \in \begin{cases} \{0\} \text{ if } n \in [0, 1), \\ [0, +\infty) \text{ if } n = 1, \\ \{+\infty\} \text{ if } n > 1, \end{cases} \quad \text{and} \quad q^\infty(r) \in \begin{cases} [0, +\infty) & \text{if } r = 0, \\ \{+\infty\} & \text{if } r > 0. \end{cases} \tag{3.9}$$

The pressure p^∞ can be viewed as a volume exclusion pressure, while the pressures $n_1^\infty q^\infty$ and $n_2^\infty q^\infty$ are segregation pressures. Eq. (3.6) suggests to decompose the domain in two parts. We consider the domain $\Omega(t) = \{x \mid p^\infty(x,t) > 0\}$ and the complementary domain, where the pressure is equal to 0. Notice that, because of Eq. (3.6), $\Omega(t) \subset \{x \mid n^\infty(x,t) = 1\}$. Moreover, the two domains coincide almost everywhere. Indeed, if $n^\infty = 1$ and $p^\infty = 0$, because of the reaction term in (3.5) the density would grow following

$$\partial_t n^\infty = n_1^\infty G_1(0) + n_2^\infty G_2(0) > 0, \tag{3.10}$$

and the total density would become greater than the maximum density. If initially the pressure $p^\infty = 0$ and the total density n^∞ is strictly smaller than 1, the total density will follow Eq. (3.10). It will grow until the value 1 is reached, and then p^∞ will become nonnegative. Thanks to the segregation property (3.7) we can decompose $\Omega(t)$ in two subdomain, $\Omega_1(t) = \Omega(t) \cap \{x \mid {n_1}^\infty(x,t) = 1\}$ and $\Omega_2(t) = \Omega(t) \cap \{x \mid {n_2}^\infty(x,t) = 1\}$. Then thanks to (3.7), $\Omega_1(t)$ and $\Omega_2(t)$ are disjoint and their union is $\Omega(t)$.

Remark 2. It is interesting to remark that

$$p_1^\infty = \begin{cases} p^\infty & \text{in } \Omega_1(t), \\ p^\infty + q^\infty & \text{in } \Omega_2(t), \\ 0 & \text{outside } \Omega(t), \end{cases} \quad \text{and} \quad p_2^\infty = \begin{cases} p^\infty + q^\infty & \text{in } \Omega_1(t), \\ p^\infty & \text{in } \Omega_2(t), \\ 0 & \text{outside } \Omega(t). \end{cases} \tag{3.11}$$

The pressure p_1^∞ is driving the movement of the density n_1^∞ which is equal to 0 on $\Omega_2(t)$. So q^∞ does not appear in the limit equation of n_1^∞. The same reasoning can be applied to n_2^∞. It shows that the pressure q^∞ does not influence the limit model. Then at the limit the dynamics of the densities n_1^∞ and n_2^∞ are driven by ∇p^∞ even though $p_1^\infty \neq p_2^\infty$.

The equation for the pressure p^∞ inside $\Omega(t)$ is deduced from the complementary relation (3.8) and reads:

$$\Delta p^\infty + n_1^\infty G_1(p^\infty) + n_2^\infty G_2(p^\infty) = 0 \text{ on } \Omega(t).$$

Thanks to (3.6), the pressure p^∞ is equal to zero on the boundary $\partial\Omega(t)$. However the normal derivative of the pressure is non-zero and controls the movement of the domain boundary. The exterior boundary is denoted by Σ and the interface between the two populations is called Γ. Knowing that in the system (2.3) - (2.6) the densities n_1 and n_2 diffuse with velocities ∇p (see Remark 2) which in the limit, is equal to ∇p^∞ respectively on Ω_1 and Ω_2, we deduce that the boundaries Σ and Γ both move in the normal direction with velocities

$$V_\Sigma = -\nabla p^\infty \quad \text{and} \quad V_\Gamma = -(\nabla p^\infty \cdot \upsilon)\upsilon, \tag{3.12}$$

where υ is any of the two opposite unit normal vectors to Γ. The velocity V_Σ is normal to Σ. Indeed, p^∞ is constant equal to zero along Σ from (3.6), so, its gradient must be in the normal direction to Σ. On the other hand, Γ does not need to be a level surface of p^∞, so ∇p^∞ must be projected along the normal direction to Γ.

To help understand the expression of the velocity (3.12) of the limit model, we now consider a particular solution of the HSM. We consider the case where the initial densities are defined by $n_1^{\text{ini}} = \mathbb{1}_{B_{R_1^{\text{ini}}}}$ and $n_2^{\text{ini}}(t,x) = \mathbb{1}_{B_{R_2^{\text{ini}}} \setminus B_{R_1^{\text{ini}}}}$ with B_R the ball of center 0 and radius R and $\mathbb{1}_S$ is the indicator function

of the set S. We suppose that $R_1^{\text{ini}} < R_2^{\text{ini}}$, then $n^{\text{ini}} = \mathbb{1}_{B_{R_2^{\text{ini}}}}$. We are looking for solutions of the HSM of the form $n_1^\infty(x,t) = \mathbb{1}_{B_{R_1(t)}(x)}$ and $n_2^\infty(x,t) = \mathbb{1}_{B_{R_2(t)}\setminus B_{R_1(t)}(x)}$ with $R_1(0) = R_1^{\text{ini}}$ and $R_2(0) = R_2^{\text{ini}}$. Thus we have $n(x,t) = \mathbb{1}_{B_{R_2(t)}}$ and so, we get:

$$\partial_t n^\infty = R_2'(t)\delta_{\{|x|=R_2(t)\}}. \tag{3.13}$$

Using Eq. (3.5) and knowing that n_1^∞, n_2^∞ are constant equal to 0 or 1, we obtain that n^∞ is solution in the sense of the distribution of

$$\partial_t n^\infty = \Delta p^\infty + n_1^\infty G_1(p^\infty) + n_2^\infty G_2(p^\infty).$$

Then for all $\varphi \in C_c^\infty(\mathbb{R}^d)$

$$\int_{\mathbb{R}^d} \partial_t n^\infty \, \varphi dx = \int_{B_{R_2(t)}} p^\infty \Delta\varphi dx + \int_{B_{R_2(t)}} \Big(n_1^\infty G_1(p^\infty) + n_2^\infty G_2(p^\infty)\Big)\varphi dx.$$

Since p^∞ verifies the complementary relation (3.8), applying the Green formula twice we get

$$\int_{\mathbb{R}^d} \partial_t n^\infty \, \varphi dx = \int_{\partial B_{R_2(t)}} p^\infty(\nabla\varphi \cdot \upsilon) d\sigma - \int_{\partial B_{R_2(t)}} (\nabla p^\infty \cdot \upsilon)\varphi d\sigma$$

where $d\sigma$ is the surface element and υ is the normal directed outward the domain $B(R_2(t))$. Using radial symmetry and knowing that the pressure p^∞ is equal to 0 at the interface, we obtain

$$\partial_t n^\infty = -\nabla p^\infty \cdot \upsilon. \tag{3.14}$$

Since $\partial B(R_2(t))$ is a level surface of the pressure p^∞, its gradient is normal to $\partial B(R_2(t))$. Then identifying Eqs. (3.13) and (3.14), we have

$$R_2'(t) = |\nabla p^\infty(R_2(t), t)|,$$

where, by abuse of notation, we have denoted $p^\infty(r,t)$ the constant value of $p^\infty(.,t)$ on the surface $\{|x| = r\}$. Similarly, applying the same result on the species n_1^∞, we obtain

$$R_1'(t) = -\nabla p^\infty(R_1(t), t) \cdot \upsilon.$$

The limit HSM is graphically represented in Figure 4.

3.2. Formal proof of Theorem 1

This section is dedicated to the formal proof of Theorem 1. First, we prove Eqs. (3.6) and (3.7) that lead to the definition of the evolving domains of the HSM. Secondly, we compute the equations for the densities n_1, n_2 and n in the limit $\epsilon \to 0, m \to +\infty$. Third, we prove Eq. (3.8), also named complementary relation, which gives the evolution of the pressure inside the domain for the HSM. Finally, we compute the speeds of the boundaries of the domains.

Proof. Eqs. (3.6) and (3.7) follow from the pressure laws (1.5) and (2.2). Indeed, since $(1-n)p_\epsilon = \epsilon n$, it follows in the limit $\epsilon \to 0$ that

$$(1 - n^\infty)p^\infty = 0.$$

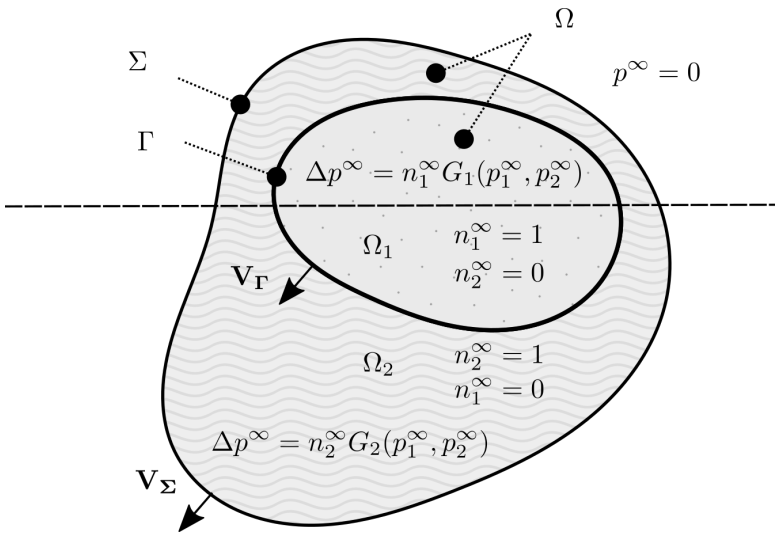

Figure 4. Graphical representation of the result exposed in Theorem 1. The grey dotted region is $\Omega_1(t)$ while the region filled with wavy lines is $\Omega_2(t)$.

Working out the repulsion pressure law (2.2) leads to the formula

$$(1+r)(\frac{m-1}{m}q_m(r)+1) = (\frac{m-1}{m}q_m(r)+1)^{\frac{m}{m-1}}.$$

Taking the limit $m \to +\infty$, we have

$$(1+r^\infty)(q^\infty+1) = q^\infty + 1$$

which implies that $r^\infty(q^\infty+1) = 0$. Since $q_m \geq 0$ for all m, we deduce $q^\infty + 1 > 0$ and

$$r^\infty = n_1^\infty n_2^\infty = 0.$$

Eqs. (3.3) and (3.4) follow directly from taking the limit $\epsilon \to 0, m \to +\infty$ and $\alpha \to 0$ in (2.3) and (2.4). To recover (3.5), it is first interesting to remark that the solution of (2.3)-(2.6) satisfies

$$\begin{aligned}\partial_t n - \Delta(H_{\epsilon,m}(n,r)) + \alpha\nabla\cdot(n_1\nabla(\Delta n_1) + n_2\nabla(\Delta n_2)) \\ = n_1 G_1(p_1) + n_2 G_2(p_2),\end{aligned} \tag{3.15}$$

where

$$H_{\epsilon,m}(n,r) = (p_\epsilon(n) - \epsilon\ln(p_\epsilon(n)+\epsilon) + \epsilon\ln\epsilon) + (rq_m(r) + (r+1)^m - q_m(r)). \tag{3.16}$$

Indeed, by adding (2.3) and (2.4), we obtain

$$\begin{aligned}\partial_t n - \nabla\cdot(n\nabla p_\epsilon(n) + 2r\nabla q_m(r) + q_m(r)\nabla r) + \alpha\nabla\cdot(n_1\nabla(\Delta n_1) + n_2\nabla(\Delta n_2)) \\ = n_1 G_1(p_1) + n_2 G_2(p_2).\end{aligned} \tag{3.17}$$

Then given formula (1.5),

$$\begin{aligned} n\nabla p_\epsilon(n) &= n\, p_\epsilon'(n)\nabla n \\ &= \epsilon\frac{n}{(1-n)^2}\nabla n \\ &= (p_\epsilon'(n) - \epsilon\frac{1}{(1-n)})\nabla n \\ &= \nabla(p_\epsilon(n) - \epsilon\ln(p_\epsilon(n)+\epsilon) + \epsilon\ln\epsilon), \end{aligned} \tag{3.18}$$

and given formula (2.2),

$$\begin{aligned} 2r\nabla q_m(r) + q_m(r)\nabla r &= r\nabla q_m(r) + \nabla(rq_m(r)) \\ &= (1+r)\nabla q_m(r) - \nabla q_m(r) + \nabla(rq_m(r)) \\ &= m(1+r)^{m-1}\nabla r + \nabla((r-1)q_m(r)) \\ &= \nabla(rq_m(r) + (r+1)^m - q_m(r)), \end{aligned} \tag{3.19}$$

and inserting (3.18), (3.19) into (3.17) gives (3.15), (3.16). Let us denote

$$h_{\epsilon,m}(x,t) = H_{\epsilon,m}(n_{\epsilon,m}(x,t), r_{\epsilon,m}(x,t))$$

and h^∞ its limit when $\epsilon \to 0, m \to \infty$. Since $(r+1)^m = (1+r)(\frac{m-1}{m}q_m(r)+1)$ and $r^\infty = 0$, passing to the limit as $\epsilon \to 0, m \to \infty$, we obtain

$$\begin{aligned} h^\infty &= p^\infty + r^\infty q^\infty + (q^\infty + 1)(1 + r^\infty) - q^\infty \\ &= p^\infty + 1. \end{aligned} \tag{3.20}$$

So at the limit, we have:

$$\partial_t n^\infty - \Delta p^\infty = n_1^\infty G_1(p_1^\infty) + n_2^\infty G_2(p_2^\infty).$$

To recover the complementary relation (3.8), we need to compute an evolution equation for the pressure. To do so, we multiply the density equation (3.15) by $p'_\epsilon(n)$ and obtain,

$$\begin{aligned} \partial_t p_\epsilon - p'_\epsilon(n)\Delta(H_{\epsilon,m}(n,r)) + \alpha p'_\epsilon(n)\nabla\cdot(n_1\nabla(\Delta n_1) + n_2\nabla(\Delta n_2)) \\ = p'_\epsilon(n)(n_1 G_1(p_1) + n_2 G_2(p_2)), \end{aligned} \tag{3.21}$$

Multiplying Eq. (3.21) by ϵ and taking into account that $p'_\epsilon(n) = \frac{1}{\epsilon}(p_\epsilon + \epsilon)^2$ yields

$$\begin{aligned} \epsilon\partial_t p_\epsilon - (p_\epsilon+\epsilon)^2\Delta(H_{\epsilon,m}(n,r)) + \alpha(p_\epsilon+\epsilon)^2\nabla\cdot(n_1\nabla(\Delta n_1) + n_2\nabla(\Delta n_2)) \\ = (p_\epsilon+\epsilon)^2(n_1 G_1(p_1) + n_2 G_2(p_2)). \end{aligned}$$

We now take the limit $\epsilon \to 0$, $m \to \infty$ and $\alpha \to 0$, and using the expression (3.20) for the limit of $H_{\epsilon,m}$, we get,

$$-p^{\infty 2}\Delta p^\infty = p^{\infty 2}(n_1 G_1(p_1) + n_2 G_2(p_2)). \tag{3.22}$$

It leads to the complementary relation (3.8).This concludes the formal proof of the theorem. □

Now, we prove Formula (3.12). We first focus on the speed of the exterior boundary Σ. Thanks to Eq. (3.5), for all $\varphi \in C_c^\infty(\mathbb{R}^d)$ and using Green's formula

$$\begin{aligned} \partial_t \int_{\mathbb{R}^d} n^\infty\,\varphi\,dx &= \int_{\mathbb{R}^d} \partial_t n^\infty\,\varphi\,dx \\ &= \int_{\mathbb{R}^d} p^\infty\Delta\varphi\,dx + \int_{\mathbb{R}^d} n_1^\infty\,G_1(p_1^\infty)\,\varphi\,dx + \int_{\mathbb{R}^d} n_2^\infty\,G_2(p_2^\infty)\,\varphi\,dx. \end{aligned}$$

Since p^∞ is equal to 0 outside $\Omega(t)$ and because n_1^∞ and n_2^∞ are both constant equal to 1 on $\Omega_1(t)$ and $\Omega_2(t)$ respectively and equal to 0 outside, we have

$$\begin{aligned} \partial_t \int_{\mathbb{R}^d} n^\infty\,\varphi\,dx = \int_{\Omega_1(t)} p^\infty\Delta\varphi\,dx + \int_{\Omega_2(t)} p^\infty\Delta\varphi\,dx \\ + \int_{\Omega_1(t)} G_1(p_1^\infty)\,\varphi\,dx + \int_{\Omega_2(t)} G_2(p_2^\infty)\,\varphi\,dx \end{aligned}$$

Therefore applying the Green formula twice, yields

$$\begin{aligned}\partial_t \int_{\mathbb{R}^d} n^\infty \varphi dx &= \int_{\Omega_1(t)} (\Delta p^\infty + G_1(p^\infty))\varphi \, dx - \int_{\partial\Omega_1(t)} \frac{\partial p^\infty}{\partial \upsilon}\varphi \, d\sigma + \int_{\partial\Omega_1(t)} p^\infty \frac{\partial \varphi}{\partial \upsilon} \, d\sigma \\ &\quad + \int_{\Omega_2(t)} (\Delta p^\infty + G_2(p^\infty))\varphi \, dx - \int_{\partial\Omega_2(t)} \frac{\partial p^\infty}{\partial \upsilon}\varphi \, d\sigma + \int_{\partial\Omega_2(t)} p^\infty \frac{\partial \varphi}{\partial \upsilon} \, d\sigma \\ &= \int_{\Omega(t)} (\Delta p^\infty + n_1^\infty G_1(p^\infty) + n_2^\infty G_2(p^\infty)) \, \varphi \, dx - \int_{\partial\Omega(t)} \frac{\partial p^\infty}{\partial \upsilon}\varphi \, d\sigma \\ &\quad - \int_{\Gamma(t)} [\frac{\partial p^\infty}{\partial \upsilon}]_{12} \, \varphi \, d\sigma + \int_{\partial\Omega(t)} p^\infty \frac{\partial \varphi}{\partial \upsilon} \, d\sigma + \int_{\Gamma(t)} [p^\infty]_{12} \frac{\partial \varphi}{\partial \upsilon} \, d\sigma, \end{aligned} \tag{3.23}$$

where υ is the unit normal vector. For $x \in \Gamma$, we denote

$$[\frac{\partial p^\infty}{\partial \upsilon}]_{12} = (\nabla(p^\infty|_{\Omega_2})(x) - \nabla(p^\infty|_{\Omega_1})(x)) \cdot \upsilon(x),$$

and

$$[p^\infty]_{12} = (p^\infty|_{\Omega_2})(x) - (p^\infty|_{\Omega_1})(x).$$

On $\partial\Omega(t)$, $\partial\Omega_1(t)$, $\partial\Omega_2(t)$ the unit normals υ are directed outwards to the respective domains. On $\Gamma(t)$, the normal υ is directed from $\Omega_2(t)$ towards $\Omega_1(t)$. From Eq. (3.8), the first integral in (3.23) is equal to 0. In addition, the pressure is equal to zero on the boundary $\partial\Omega(t)$ so that

$$\begin{aligned}\partial_t \int_{\mathbb{R}^d} n^\infty \, \varphi \, dx &= \partial_t \int_{\Omega(t)} n^\infty \, \varphi \, dx \\ &= - \int_{\partial\Omega(t)} \frac{\partial p^\infty}{\partial \upsilon}\varphi \, d\sigma - \int_{\Gamma(t)} [\frac{\partial p^\infty}{\partial \upsilon}]_{12} \, \varphi \, d\sigma + \int_{\Gamma(t)} [p^\infty]_{12} \frac{\partial \varphi}{\partial \upsilon} \, d\sigma. \end{aligned} \tag{3.24}$$

Moreover since $n^\infty = 1$ in the domain $\Omega(t)$, we have

$$\partial_t (\int_{\Omega(t)} n^\infty \, \varphi \, dx) = \int_{\partial\Omega(t)} (V_{\partial\Omega(t)} \cdot \upsilon) \, n^\infty \, \varphi \, d\sigma, \tag{3.25}$$

where $V_{\partial\Omega(t)}$ is the speed of the boundary $\partial\Omega(t)$ and is directed along the normal υ in the outwards direction. Since Eqs. (3.24) and (3.25) are verified for all $\varphi \in C_c^\infty(\mathbb{R}^d)$, we deduce that

$$V_{\partial\Omega(t)} = -\frac{\partial p^\infty}{\partial \upsilon}\upsilon = -(\nabla p^\infty \cdot \upsilon)\upsilon, \tag{3.26}$$

and at the interface Γ,

$$[p^\infty]_{12} = 0 \quad \text{and} \quad [\frac{\partial p^\infty}{\partial \upsilon}]_{12} = 0. \tag{3.27}$$

Then, both p^∞ and its normal derivative are continuous at the interface Γ. Since p^∞ is equal to zero along $\partial\Omega$, its gradient is normal to $\partial\Omega$ and the velocity on the outer domain given by (3.26) can be rewritten

$$V_{\partial\Omega(t)} = -\nabla p^\infty.$$

To find the velocity at the interface the same method needs to be applied on either n_1^∞ or n_2^∞ and it leads to

$$V_{\Gamma(t)} = -(\nabla p^\infty \cdot \upsilon)\upsilon, \tag{3.28}$$

where $V_{\Gamma(t)}$ is the speed of the boundary $\Gamma(t)$. This gives (3.12).

3.3. Numerical validation

3.3.1. Analytical solution of the Hele-Shaw model

The HSM is characterised by the complementary relation (3.8) and the velocity of the boundary given by (3.12). In the one-dimensional case (1D), the solution of this problem can be computed explicitely. We will consider $G(p) = g(p^* - p)$, with p^* the maximum pressure and g the growth rate, since it is one of the most common growth terms in the literature [16, 17, 18]. In the case of a single population, the complementary relation (3.8) in 1D can be rewritten as

$$-p''(x) + gp = gp^* \text{ on } \Omega(t). \tag{3.29}$$

The solutions of this problem are of the form

$$p(x) = Ae^{\sqrt{g}x} + Be^{-\sqrt{g}x} + p^*,$$

with constants A, B depending on the boundary conditions. We compute the exact solution in two different cases which are going to be used for the numerical validation of the model.

Example 1 We first consider the case where the two species have the same growth term

$$G_1(p) = G_2(p) = g(p^* - p), \tag{3.30}$$

with one species surrounded by the other one. The density n_2^{ini} is defined as the indicator function of $[x_{\Gamma^-}^{\text{ini}}; x_{\Gamma^+}^{\text{ini}}]$ and the density n_1^{ini} is defined as the indicator function of $[x_{\Sigma^-}^{\text{ini}}; x_{\Sigma^+}^{\text{ini}}] \setminus [x_{\Gamma^-}^{\text{ini}}; x_{\Gamma^+}^{\text{ini}}]$ where $x_{\Gamma^-}^{\text{ini}}, x_{\Gamma^+}^{\text{ini}}$ represents the interfaces between the two populations and $x_{\Sigma^-}^{\text{ini}}, x_{\Sigma^+}^{\text{ini}}$ represent the exterior boundaries of the support of the total density. More specifically,

$$n_1^{\text{ini}}(x) = \mathbb{1}_{[x_{\Sigma^-}^{\text{ini}}; x_{\Gamma^-}^{\text{ini}}]}(x) + \mathbb{1}_{[x_{\Gamma^+}^{\text{ini}}; x_{\Sigma^+}^{\text{ini}}]}(x) \quad \text{and} \quad n_2^{\text{ini}}(x) = \mathbb{1}_{[x_{\Gamma^-}^{\text{ini}}; x_{\Gamma^+}^{\text{ini}}]}(x). \tag{3.31}$$

Since the two populations have the same growth function, the complementary relation can be treated as that of a single population of cells (3.29) with the boundary conditions $p(x_{\Sigma^-}) = 0$ and $p(x_{\Sigma^+}) = 0$ at any time. A simple computation shows that

$$p(x) = p^*\Big(1 - \frac{\cosh(\sqrt{g}(\frac{x_{\Sigma^-}+x_{\Sigma^+}}{2} - x)}{\cosh(\sqrt{g}\frac{x_{\Sigma^-}-x_{\Sigma^+}}{2})}\Big),$$

where cosh and sinh stand for the hyperbolic cosine and sine. The velocities of the exterior boundaries and of the interfaces can be easily computed:

$$V_{\Sigma^-} = -p^*\sqrt{g}\frac{\sinh(\sqrt{g}\frac{x_{\Sigma^-}-x_{\Sigma^+}}{2})}{\cosh(\sqrt{g}\frac{x_{\Sigma^-}-x_{\Sigma^+}}{2})} \quad \text{and} \quad V_{\Sigma^+} = p^*\sqrt{g}\frac{\sinh(\sqrt{g}\frac{x_{\Sigma^-}-x_{\Sigma^+}}{2})}{\cosh(\sqrt{g}\frac{x_{\Sigma^-}-x_{\Sigma^+}}{2})},$$

and

$$V_{\Gamma^-} = p^*\sqrt{g}\frac{\sinh(\sqrt{g}(\frac{x_{\Sigma^-}+x_{\Sigma^+}}{2} - x_{\Gamma^-})}{\cosh(\sqrt{g}\frac{x_{\Sigma^-}-x_{\Sigma^+}}{2})} \quad \text{and} \quad V_{\Gamma^+} = p^*\sqrt{g}\frac{\sinh(\sqrt{g}(\frac{x_{\Sigma^-}+x_{\Sigma^+}}{2} - x_{\Gamma^+})}{\cosh(\sqrt{g}\frac{x_{\Sigma^-}-x_{\Sigma^+}}{2})}.$$

Then $x_{\Sigma^\pm}$ and $x_{\Gamma^\pm}$ evolve respectively according to $\frac{d}{dt}x_{\Sigma^\pm} = V_{\Sigma^\pm}$ and $\frac{d}{dt}x_{\Gamma^\pm} = V_{\Gamma^\pm}$. Since initially $x_{\Sigma^-}^{\text{ini}} < x_{\Gamma^-}^{\text{ini}} < x_{\Gamma^+}^{\text{ini}} < x_{\Sigma^+}^{\text{ini}}$, the velocities V_{Σ^-},V_{Γ^-} are nonpositive and the velocities V_{Σ^+},V_{Γ^+} are nonnegative. It means that the densities n_1 and n_2 spread. However $|V_{\Gamma^-}| \leq V_{\Sigma^-}$ and $|V_{\Gamma^+}| \leq V_{\Sigma^-}$ so the interface is moving more slowly than the exterior boundary. This means that the density n_1 is not only transported but also spreads. The density n_2 spreads and simultaneously pushes n_1.

Example 2 We now consider two species having only one contact point, with different growth terms

$$G_1(p) = g_1(p_1^* - p) \quad \text{and} \quad G_2(p) = g_2(p_2^* - p). \tag{3.32}$$

The initial densities are defined as indicator functions of $[x_{\Sigma^-}^{\text{ini}}; x_\Gamma^{\text{ini}}]$ and $[x_\Gamma^{\text{ini}}; x_{\Sigma^+}^{\text{ini}}]$ where $x_{\Sigma^-}^{\text{ini}}, x_{\Sigma^+}^{\text{ini}}$ define the boundaries of the support of the total density and x_Γ^{ini} defines the interface between the supports of the two densities. More specifically,

$$n_1^{\text{ini}}(x) = \mathbb{1}_{[x_{\Sigma^-}^{\text{ini}}; x_\Gamma^{\text{ini}}]}(x) \quad \text{and} \quad n_2^{\text{ini}}(x) = \mathbb{1}_{[x_\Gamma^{\text{ini}}; x_{\Sigma^+}^{ini}]}(x). \tag{3.33}$$

The pressure follows the complementary relation (3.8), which can be rewritten as

$$\begin{cases} -p''(x) + g_1 p = g_1 p_1^* \text{ in } \Omega_1 = [x_{\Sigma^-}; x_\Gamma], \\ -p''(x) + g_2 p = g_2 p_2^* \text{ in } \Omega_2 = [x_\Gamma; x_{\Sigma^+}], \end{cases}$$

with the additional conditions $p(x_{\Sigma^-}) = 0$, $p(x_{\Sigma^+}) = 0$, and p and p' are continuous at x_Γ. After some computations we find,

$$p(x) = \begin{cases} 2A_1 e^{\sqrt{g_1} x_{\Sigma^-}} \sinh(\sqrt{g_1}(x - x_{\Sigma^-})) + p_1^*(1 - e^{-\sqrt{g_1}(x - x_{\Sigma^-})}) & \text{in } [x_{\Sigma^-}; x_\Gamma], \\ 2A_2 e^{\sqrt{g_2} x_{\Sigma^+}} \sinh(\sqrt{g_2}(x - x_{\Sigma^+})) + p_1^*(1 - e^{-\sqrt{g_2}(x - x_{\Sigma^+})}) & \text{in } [x_\Gamma; x_{\Sigma^+}], \\ 0 \quad \text{in } (-\infty, x_{\Sigma^-}] \cup [x_{\Sigma^+}, +\infty), \end{cases}$$

with

$$\begin{aligned} A_1 = \tfrac{e^{\sqrt{g_2} x_{\Sigma^-}}}{D}(\quad & p_1(\sqrt{g_2}(1 - e^{-\sqrt{g_1} * (x_\Gamma - x_{\Sigma^+})}) \cosh(\sqrt{g_2}(x_\Gamma - x_{\Sigma^-})) \\ & - \sqrt{g_1} e^{-\sqrt{g_2}(x_\Gamma - x_{\Sigma^+})} \sinh(\sqrt{g_2}(x_\Gamma - x_{\Sigma^-}))) \\ & + p_2 \sqrt{g_2}(-(1 - e^{-\sqrt{g_2}(x_\Gamma - x_{\Sigma^-})}) \cosh(\sqrt{g_2}(x_\Gamma - x_{\Sigma^-})) \\ & + e^{-\sqrt{g_2}(x_\Gamma - x_{\Sigma^-})} \sinh(\sqrt{g_2}(x_\Gamma - x_{\Sigma^-})))), \end{aligned}$$

and

$$\begin{aligned} A_2 = \tfrac{e^{\sqrt{g_1} x_{\Sigma^+}}}{D}(\quad & p_1 \sqrt{g_1}((1 - e^{-\sqrt{g_1}(x_\Gamma - x_{\Sigma^-})}) \cosh(\sqrt{g_1}(x_\Gamma - x_{\Sigma^-})) \\ & - e^{-\sqrt{g_1}(x_\Gamma - x_{\Sigma^-})} \sinh(\sqrt{g_1}(x_\Gamma - x_{\Sigma^-}))) \\ & + p_2(\sqrt{g_2}(1 - e^{-\sqrt{g_2}(x_\Gamma - x_{\Sigma^+})}) \cosh(\sqrt{g_2}(x_\Gamma - x_{\Sigma^+})) \\ & - \sqrt{g_1} e^{-\sqrt{g_2}(x_\Gamma - x_{\Sigma^+})} \sinh(\sqrt{g_1}(x_\Gamma - x_{\Sigma^-})))). \end{aligned}$$

From this expressions we can compute the speeds of the exterior boundary and of the interface by computing the derivative of the pressure and evaluating it at $x_{\Sigma^-}^{\text{ini}}$, $x_{\Sigma^+}^{\text{ini}}$ and x_Γ^{ini}.

3.3.2. Numerical validation

In this section we use the numerical scheme presented in Section 4 to illustrate that the solution of the SPM converges to the corresponding solution of the HSM described in Section 3.1. In order to facilitate the comparison with the analytical solutions of the HSM shown in the previous section, the simulations are performed in one dimension. To compare the two models we initialize them with the same initial configuration: the densities are taken as segregated indicator functions. We consider the two different cases with different growth functions and different initial conditions, corresponding to Examples 1 and 2 of Section 3.2. For Example 1, we plot the simulation for one set of parameters: $\epsilon = 0.1$, $m = 10$, $\alpha = 0.01$ and $\nu = 0.001$ (where ν is introduced for the RSPM in Section 4). For

Example 2, we plot the simulation for a set of parameters: $(\epsilon, m, \alpha, \nu) = (1, 2, 0.1, 0.01)$, $(\epsilon, m, \alpha, \nu) = (0.1, 10, 0.01, 0.001)$, $(\epsilon, m, \alpha, \nu) = (0.02, 50, 0.001, 0.0001)$.

The first case defined as Example 1 in Section 3.2 is illustrated in Figure 5. We use the growth function (3.30) with the parameters $g = 1$ and $p^* = 10$. The boundary and interface are taken as $x^{\text{ini}}_{\Sigma^\pm} = \pm 1.4$ and $x^{\text{ini}}_{\Gamma^\pm} = \pm 0.6$. Then the initial density of the HSM are defined by Eq. (3.31). As initial conditions of the SPM, we take

$$n_1^{\text{ini}}(x) = 0.98\ (\mathbb{1}_{[-1.4;-0.6]}(x) + \mathbb{1}_{[0.6;1.4]}(x)) \quad \text{and} \quad n_2^{\text{ini}}(x) = 0.98\ \mathbb{1}_{[-0.6;0.6]}(x). \tag{3.34}$$

We take $n_1 = n_2 = 0.98$ initially as it is close to the singular value 1. We plot the numerical solutions of the SPM (solid line) and of the HSM (dashed line) on the same figure. The species n_1 and n_2 are plotted in red and blue, respectively. In this example the solution of the SPM is expected to be close to the particular solution of the HSM given in Example 1.

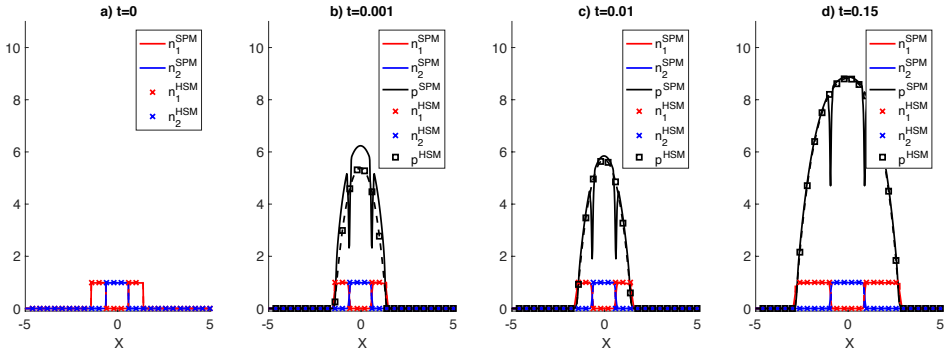

Figure 5. Snapshots of densities n_1 (red), n_2 (blue) and pressure p (black) for SPM (solid line) and HSM (dashed line with marker) for Example 1 at different times: (a) $t = 0$, (b) $t = 0.001$, (c) $t = 0.01$, (d) $t = 0.15$. Initial conditions: density of the SPM from Eq. (3.34), density of the HSM from Eq. (3.31), growth functions from Eq. (3.30).

In Figures 5, panel (a) is for the initial configuration and panels (b), (c), (d) are for times $t = 0.001$, $t = 0.01$, $t = 0.15$ respectively. First of all, we notice that the approximation is excellent except for the pressure at small times, and at the interface between the two cell population. While the pressure of the HSM is smooth wherever the total density is positive, the pressure of the SPM exhibits sharp ditches at the interfaces between the two populations. These ditches appear because of the fourth order term in the model (2.3)-(2.6). Indeed, because of the fourth order term, n_1 and n_2 are continuous. Since n_1 is zero in Ω_1 and n_2 is zero in Ω_1, both are zero at the interface and since they are continuous, they are both very small in a small vicinity of the interface. Therefore the repulsion pressure p is also small at the interface. Since the width of the the interface is of the order of alpha and is very small, this implies that the region of small pressure is very narrow and generates a sharp ditch near the interface. Away from the interface, the pressure does not feel the influence of the fourth order term because all densities are smooth and therefore, it approximates very well the pressure given by the HSM model. Away from the interfaces, the pressures given by the two models are similar except at small times. In Figure 5(b), the pressure of the SPM is larger than that of the HSM. However, we do not observe any influence of this difference on the densities. On Figures 5(c) and 5(d), the two pressures are almost the same for the two models. Overall, the dynamics of the SPM and the HSM are quite similar. In Figure 5, we observe that the blue (inner) species pushes the red (outer) species in order to be allowed to grow.

The second case is illustrated in Figure 6. The growth functions are defined by (3.32) with the parameters $g_1 = g_2 = 1$, $p_1^* = 20$ and $p_2^* = 10$. As initial conditions of the SPM we take

$$n_1^{\text{ini}}(x) = 0.98\ \mathbb{1}_{[x_{\Sigma^-}^{\text{ini}}; x_\Gamma^{\text{ini}}]}(x) \quad \text{and} \quad n_2^{\text{ini}}(x) = 0.98\ \mathbb{1}_{[x_\Gamma^{\text{ini}}; x_{\Sigma^+}^{\text{ini}}]}(x), \tag{3.35}$$

where $x_{\Sigma^\pm}^{\text{ini}} = \pm 1.4$ and $x_\Gamma^{\text{ini}} = 0$. The initial density of the HSM are defined with formula (3.33). In this example, we plot the solution of the HSM (dashed line) in Figure 6 (i) and the solution of the SPM (solid line) in Figure 6 (ii)-(iv) (respectively for the parameters $(\epsilon, m, \alpha, \nu) = (1, 2, 0.1, 0.01)$, $(\epsilon, m, \alpha, \nu) = (0.1, 10, 0.01, 0.001)$, $(\epsilon, m, \alpha, \nu) = (0.02, 50, 0.001, 0.0001)$). For each line, panels (a), (b), (c) are for times $t = 0.001$, $t = 0.01$, $t = 0.15$. Panel (d) is also a plot at time $t = 0.15$, but only of the densities. The species n_1 and n_2 are plotted in red and blue, respectively and the pressure p is plotted in black.

In Figure 6 (i)-(iv), the red species (leftmost) which has the biggest growth rate pushes the blue species (rightmost) toward the right. Therefore by growing more rapidly, the red species exerts a bigger pressure on the blue species than the blue species exerts on the red species. This pressure imbalance which is visible on Figure 6 (a)-(c), triggers the motion of the interface towards regions of lower pressure.

In Figures 6, while going from line (ii) to (iv) (which corresponds to having $\epsilon \to 0$ and $m \to \infty$), we observe three important phenomena. As seen previously in Figures 5, for small times the pressure p of the SPM and the HSM are different. However this difference is much bigger in Figures 6 (ii-a) when $(\epsilon, m, \alpha, \nu) = (1, 2, 0.1, 0.01)$ than for the two other cases. So as the parameters ϵ, m converge, the time for the two models to provide similar solutions reduces. This corresponds to an initial layer converging faster to the initial state of the HSM. The other main difference is the pressure ditch at the interface as shown in Figures 6 (a), (b), (c). As ϵ and m converge, the ditch becomes deeper. Indeed, as ϵ and m converge, the variations of n_1 and n_2 near the interface become sharper. Since the pressure near the interface is a function of the densities, its variations become sharper as well, which is consistent with the observation that the pressure ditch becomes more pronounced as these parameters converge. Except near the interface, the pressure p of the SPM and the HSM almost coincide in Figures 6 (b), (c). The last phenomenon we observe is the convergence of the densities of the SPM to the Heaviside functions which characterize the solutions of hte HSM in Figure 6 (d). Indeed as ϵ gets smaller (and m gets bigger), the fronts of the densities become steeper and the upper bounds of the densities get closer to 1.

3.3.3. Discussion

The results of the simulations presented in Figures 5 and 6 show that the dynamics of the two models are almost identical after some time. However, at the beginning of the simulation we observe some differences between the pressure of the SPM and of the HSM. This is because the initial conditions of the SPM are not well-prepared for the limit model, which generates an initial layer whose function is to relax the initial conditions to well-prepared ones. Indeed, initially in the SPM, the densities are taken as indicator functions, so at the start the pressure p_ϵ of the SPM is also an indicator function whereas that of the HSM is continuous. It takes an initial transient for the model to smooth it out, and then the two pressures coincide. In addition, the initial value of the SPM in these simulations is fixed to 98% of the packing density 1. At the beginning of the simulation, the dynamics of the SPM is driven by the

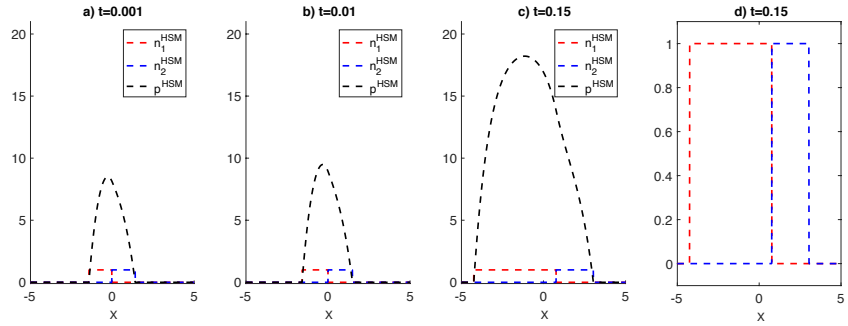

(a) Solution of the HSM

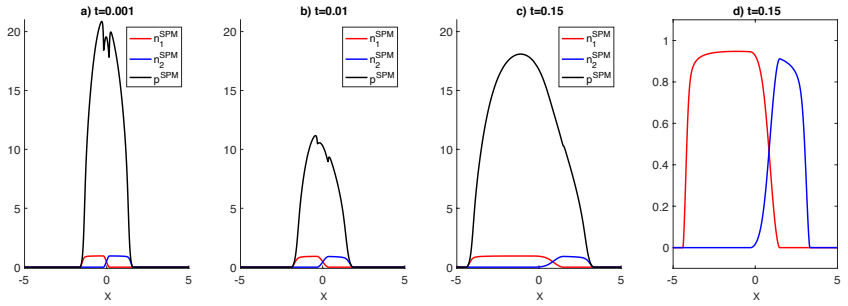

(b) Solution of the SPM with $(\epsilon, m) = (1, 2, 0.1, 0.01)$

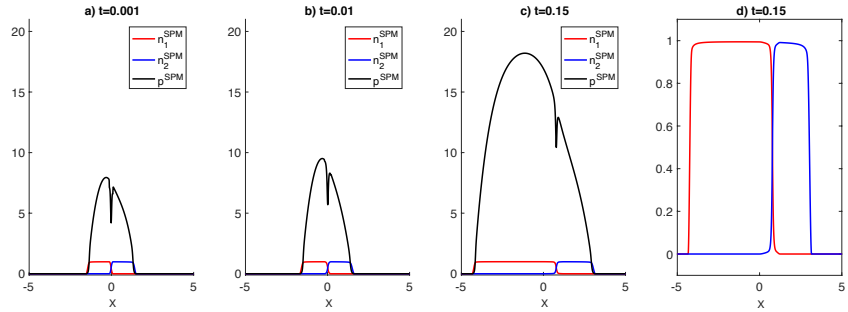

(c) Solution of the SPM with $(\epsilon, m) = (0.1, 10, 0.01, 0.001)$

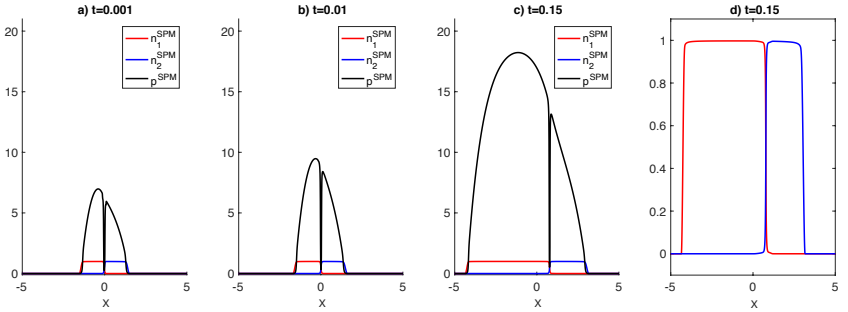

(d) Solution of the SPM with $(\epsilon, m) = (0.02, 50, 0.001, 0.0001)$

Figure 6. Snapshots of densities n_1 (red), n_2 (blue) and pressure p (black) for SPM (solid line) and HSM (dashed line) from Example 2 at different times: (a) $t = 0.01$, (b) $t = 0.01$, (c) $t = 0.15$. On panels (d) close-ups of the densities of (c) at $t = 0.15$ are plotted. Initial conditions: density of the SPM from Eq. (3.35), density of the HSM from Eq. (3.33), growth functions from Eq. (3.32).

growth terms which increase the densities to their upper bound values $n_M = p_\epsilon^{-1}(p^*) = \frac{p^*}{\epsilon+p^*} < 1$ with $p^* = \max(p_1^*, p_2^*)$ (see (3.2)). Until the densities reach their upper bound value, the SPM and the HSM are not close to each other. After this short period, we observe that the pressures of the two models fit well. It also seems that this time becomes smaller when the parameters are closer to convergence, which is consistent with the fact that initial transients are faster when the perturbation parameters are closer to their limit values.

The major difference between the two models is at the interfaces between the two populations. As a result of the fourth order terms, the densities of the SPM are not perfectly segregated and overlap only in a narrow spatial interval. As long ϵ and m are finite, the densities n_1 and n_2, which are continuous, are small in the vicinity of the interface. This creates sharp ditches in the pressures (which in this regime are function of the densities). In the limit $\epsilon \to 0$, $m \to +\infty$ and $\alpha \to 0$, the densities become discontinuous and the pressure ditches become narrower and narrower until they disappear completely. For finite ϵ and m close to the limit, despite the pressure ditches, the interface and boundary speeds are very close in the two models. These are quite remarkable results, considering that the parameters used in the tests were not yet in the asymptotic ranges where the two models should be identical.

However, it is important to remark that the comparisons between the SPM and the HSM can only be made in the case of initially segregated populations. This is necessary to initialize the free boundary model. In the case of mixed population, simulations of the SPM have been made and can be found in Section 2. They confirm the convergence of the SPM towards a free boundary model since we observe that the system self-organizes into separated domains containing the different populations. However we cannot study the convergence towards the HSM since we do not know beforehand which initial conditions for the HSM will correspond to the converged SPM.

4. Numerical method

This section is devoted to the derivation of the numerical scheme used to perform the simulations of the SPM presented in Sections 2 and 3. Since the equations for the densities are of fourth order, we first introduce a relaxation model, in which the fourth order terms are replaced by a coupled system of second order equations. Then, we present the numerical scheme together with some of its properties and derive a CFL stability condition.

4.1. Relaxation model

In order to simplify the computation of system (2.3) - (2.6), we lower its order through a suitable relaxation approximation. The relaxation system, depending on the relaxation parameter ν, is written as follows

$$\partial_t n_1^\nu - \nabla \cdot (n_1^\nu \nabla p_1^\nu) + \frac{1}{\nu} \nabla \cdot (n_1^\nu \nabla (c_1^\nu - n_1^\nu)) = n_1^\nu G_1(p_1^\nu), \tag{4.1}$$

$$\partial_t n_2^\nu - \nabla \cdot (n_2^\nu \nabla p_2^\nu) + \frac{1}{\nu} \nabla \cdot (n_2^\nu \nabla (c_2^\nu - n_2^\nu)) = n_2^\nu G_2(p_2^\nu), \tag{4.2}$$

$$\alpha \Delta c_1^\nu = \frac{1}{\nu}(c_1^\nu - n_1^\nu), \tag{4.3}$$

$$\alpha \Delta c_2^\nu = \frac{1}{\nu}(c_2^\nu - n_2^\nu). \tag{4.4}$$

with p_1 and p_2 given by the constitutive laws (2.5)-(2.6) and where c_1 and c_2 are two new variables. The fourth order terms in (2.3) - (2.6) are now replaced by second order terms supplemented with Poisson equations which define c_1 and c_2. This relaxation method has been introduced for the numerical approximation of the Navier-Stokes-Korteweg equations [39, 40]. This system is referred to as Relaxation Segregation Pressure Model (RSPM). It formally converges toward the SPM when $\nu \to 0$. Here we give supporting elements for this statement. We suppose that (n_1^ν) and (n_2^ν) converge when ν goes to 0. Since the two species play the same role, we only consider n_1. Inserting (4.3) in (4.1) we have,

$$\partial_t n_1^\nu - \nabla \cdot (n_1^\nu \nabla p_1^\nu) + \alpha \nabla \cdot (n_1^\nu \nabla \Delta c_1^\nu) = n_1^\nu G_1(p_1^\nu).$$

Then to prove the convergence we need to show that $c_1^\nu \to n_1$ when $\nu \to 0$. We can rewrite (4.3) as

$$-\alpha\Delta(c_1^\nu - n_1^\nu) + \frac{1}{\nu}(c_1^\nu - n_1^\nu) = \alpha \Delta n_1^\nu.$$

So that

$$c_1^\nu - n_1^\nu = \alpha(-\alpha\Delta + \frac{1}{\nu})^{-1}\Delta n_1^\nu.$$

Using Fourier transform, we obtain:

$$\hat{c}_1^\nu - \hat{n}_1^\nu = -\frac{\alpha|\xi|^2}{\alpha|\xi|^2 + \frac{1}{\nu}}\hat{n}_1^\nu \quad \forall \xi.$$

And then,

$$\lim_{\nu \to 0} (c_1^\nu - n_1^\nu) = 0.$$

With the same computation we can obtain that

$$\lim_{\nu \to 0} (c_2^\nu - n_2^\nu) = 0.$$

This formally shows the convergence of the RSPM toward the SPM.

4.2. The scheme

We aim to numerically solve the RSPM given by (4.1)-(4.4) with Neumann boundary conditions by a finite-volume method. The choice of the boundary condition is arbitrary because we are interested in the dynamics of the system whilst the densities have not reached the boundary. To facilitate the comprehension, we omit the indices ν. For the sake of simplicity, we only consider the 1D case on a finite interval $\Omega = (a, b)$.

We divide the computational domain into finite-volume cells $C_j = [x_{j-1/2}, x_{j+1/2}]$ of uniform size Δx with $x_j = j\Delta x$, $j \in \{1, ..., M_x\}$, and $x_j = \frac{x_{j-1/2}+x_{j+1/2}}{2}$ so that

$$a = x_{1/2} < x_{3/2} < ... < x_{j-1/2} < x_{j+1/2} < ... < x_{M_x-1/2} < x_{M_x+1/2} = b$$

and define the cell average of functions $n_1(t, x)$ and $n_2(t, x)$ on the cell C_j by

$$\bar{n}_{\beta,j}(t) = \frac{1}{\Delta x}\int_{C_j} n_\beta(t, x)\, dx, \quad \beta \in \{1, 2\}.$$

A semi-discrete finite-volume scheme is obtained by integrating system (4.1)-(4.4) over C_j and is given by

$$\begin{aligned}
\partial_t \bar{n}_{1,j}(t) &= -\frac{F_{1,j+1/2}(t) - F_{1,j-1/2}(t)}{\Delta x} + \bar{n}_{1,j}(t) G_1(p_{1,j}(t)),\\
\partial_t \bar{n}_{2,j}(t) &= -\frac{F_{2,j+1/2}(t) - F_{2,j-1/2}(t)}{\Delta x} + \bar{n}_{2,j}(t) G_2(p_{2,j}(t)),\\
\alpha \frac{c_{1,j+1}(t) - 2c_{1,j}(t) + c_{1,j-1}(t)}{(\Delta x)^2} &- \frac{1}{\nu}(c_{1,j}(t) - \bar{n}_{1,j}(t)) = 0,\\
\alpha \frac{c_{2,j+1}(t) - 2c_{2,j}(t) + c_{2,j-1}(t)}{(\Delta x)^2} &- \frac{1}{\nu}(c_{2,j}(t) - \bar{n}_{2,j}(t)) = 0.
\end{aligned} \tag{4.5}$$

Here, $c_{\beta,j}(t) \approx c_\beta(t, x_j)$, $\beta \in \{1, 2\}$ and $F_{\beta,j+1/2}$ are numerical fluxes approximating $-n_\beta u_\beta := -n_\beta \partial_x(p_\beta - \frac{1}{\nu}(c_\beta - n_\beta))$ and defined by the following upwind scheme:

$$F_{\beta,j+1/2} = (u_{\beta,j+1/2})^+ \bar{n}_{\beta,j} + (u_{\beta,j+1/2})^- \bar{n}_{\beta,j+1}, \quad \beta \in \{1, 2\}, \tag{4.6}$$

where

$$u_{\beta,j+1/2} = -\frac{(p_{\beta,j+1} - \frac{1}{\nu}(c_{\beta,j+1} - \bar{n}_{\beta,j+1})) - (p_{\beta,j} - \frac{1}{\nu}(c_{\beta,j} - \bar{n}_{\beta,j}))}{\Delta x}, \tag{4.7}$$

and $(u_{\beta,j+1/2})^+ = \max(u_{\beta,j+1/2}, 0)$ and $(u_{\beta,j+1/2})^- = \min(u_{\beta,j+1/2}, 0)$ are its positive and negative part, respectively. The numerical pressure $p_{\beta,j+1}$ for $\beta = 1, 2$ are computed applying (2.5)-(2.6) to the $\bar{n}_{\beta,j}$.

It is easy to see that scheme (4.5)–(4.7) is first order in space and if one uses an explicit Euler method for time evolution, then the scheme is also first order in time. Higher order approximations can also be obtained, see e.g. [41].

4.3. CFL condition and properties of the scheme

In this section, we present some properties of the scheme. We prove that for all times $t \geq 0$, it preserves the non-negativity of the computed densities $\bar{n}_1$ and $\bar{n}_2$ and also ensures that the total density $\bar{n}$ stays below 1. The former property guarantees physically meaningful values of the computed densities while the second one is needed to make sense of the pressure law which blows up when $\bar{n} \to 1$.

We consider the semi-discrete finite volume scheme (4.5)–(4.7) and evolve it in time by the forward Euler method. We denote by $\bar{n}^k_{1,j}$, $\bar{n}^k_{2,j}$, $p^k_{1,j}$ and $p^k_{2,j}$ the computed densities and pressures obtained at time $t^k = t^{k-1} + \Delta t^k$, i.e., $\bar{n}^k_{1,j} := \bar{n}_{1,j}(t^k)$, $\bar{n}^k_{2,j} := \bar{n}_{2,j}(t^k)$, $p^k_{1,j} := p_{1,j}(t^k)$ and $p^k_{2,j} := p_{2,j}(t^k)$, and prove the following two propositions.

Proposition 1. *(Positivity of the density) Consider the semi-discrete finite volume scheme* (4.5)–(4.7) *that is evolved in time by the forward Euler method. Provided that the initial densities* $\bar{n}^0_{1,j} \geq 0$ *and* $\bar{n}^0_{2,j} \geq 0$ *for all* $j \in \{1, ..., M_x\}$*, and that the growth terms* G_β *are nonnegative for* $\beta = \{1, 2\}$*, a sufficient CFL condition for the cell averages* $\bar{n}^k_{1_j}$ *and* $\bar{n}^k_{2_j}$*, with* $k \in [0, N_{it}]$*, to be positive is*

$$\Delta t^{k+1} \leq \frac{\Delta x}{2 \max\limits_{\substack{j\in\{1,...,M_x\},\\ \beta\in\{1,2\}}} \{(u^k_{\beta,j+1/2})^+, -(u^k_{\beta,j+1/2})^-\}}, \quad \forall k \in [0, N_{it}], \tag{4.8}$$

where $(u^k_{\beta,j+1/2})^+ := (u_{\beta,j+1/2})^+(t^k)$ *and* $(u^k_{\beta,j+1/2})^- := (u_{\beta,j+1/2})^-(t^k)$.

Proof. Assume that at a given time t^k, $\bar{n}^k_{1,j} \geq 0$ and $\bar{n}^k_{2,j} \geq 0$ for all $j \in \{1, ..., M_x\}$. Then, the new densities are given by the general formula

$$\bar{n}^{k+1}_{\beta,j} = \bar{n}^k_{\beta,j} - \frac{\Delta t^{k+1}}{\Delta x}(F^k_{\beta,j+1/2} - F^k_{\beta,j-1/2}) + \Delta t^{k+1}\, \bar{n}^k_{\beta,j} G_1(p^k_{\beta,j}) \tag{4.9}$$

where $F^k_{\beta,j+1/2} := F_{\beta,j+1/2}(t^k)$. Taking into account formula (4.6) for fluxes $F^k_{\beta,j+1/2}$ and the fact that the growth terms G_β are nonnegative for $\beta = 1, 2$, we obtain

$$\begin{aligned}
\bar{n}^{k+1}_{\beta,j} \geq & \bar{n}^k_{\beta,j} - \frac{\Delta t^{k+1}}{\Delta x}\left[(u^k_{\beta,j+1/2})^+ \bar{n}^k_{\beta,j} + (u^k_{\beta,j+1/2})^- \bar{n}^k_{\beta,j+1} - (u^k_{\beta,j-1/2})^+ \bar{n}^k_{\beta,j-1} - (u^k_{\beta,j-1/2})^- \bar{n}^k_{\beta,j}\right] \\
\geq & \frac{\Delta t^{k+1}}{\Delta x}(u^k_{\beta,j-1/2})^+ \bar{n}^k_{\beta,j-1} + \left(\frac{1}{2} - \frac{\Delta t^{k+1}}{\Delta x}(u^k_{\beta,j+1/2})^+\right)\bar{n}^k_{\beta,j} \\
& + \left(\frac{1}{2} + \frac{\Delta t^{k+1}}{\Delta x}(u^k_{\beta,j-1/2})^-\right)\bar{n}^k_{\beta,j} - \frac{\Delta t^{k+1}}{\Delta x}(u^k_{\beta,j+1/2})^- \bar{n}^k_{\beta,j+1}.
\end{aligned}$$

By definition, $(u^k_{\beta,j+1/2})^- \leq 0$ and $(u^k_{\beta,j+1/2})^+ \geq 0$ for all $j \in \{1, ..., M_x\}$. Then, provided that the CFL condition (4.8) is satisfied,

$$\frac{1}{2} - \frac{\Delta t^{k+1}}{\Delta x}(u^k_{\beta,j+1/2})^+ \geq 0 \quad \text{and} \quad \frac{1}{2} + \frac{\Delta t^{k+1}}{\Delta x}(u^k_{\beta,j-1/2})^- \geq 0 \quad \forall j \in \{1, ..., M_x\}.$$

Since $(\bar{n}^k_{1,j})_{j\in\{1,...,M_x\}}, (\bar{n}^k_{2,j})_{j\in\{1,...,M_x\}}$ are non-negative, we conclude that $\bar{n}^{k+1}_{1,j} \geq 0$ and $\bar{n}^{k+1}_{2,j} \geq 0$ for all $j \in \{1, ..., M_x\}$. □

Proposition 2. *(Maximum total density) Consider the semi-discrete finite volume scheme* (4.5)–(4.7) *that is evolved in time by the forward Euler method. Provided that the initial total density* $\bar{n}^0_j = \bar{n}^0_{1,j} + \bar{n}^0_{2,j} < 1$ *for all* $j \in \{1, ..., M_x\}$*, a sufficient CFL condition for the average total densities* $\bar{n}^k_j = \bar{n}^k_{1,j} + \bar{n}^k_{2,j}$*, to be below 1 for all* $k \in [0, N_{it}]$ *is*

$$\Delta t^{k+1} \leq \left(\frac{1}{\max\limits_{\substack{j\in\{1,...,M_x\},\\ \beta\in\{1,2\}}} \bar{n}^k_{\beta_j}} - 1\right) \frac{1}{\frac{4}{\Delta x}\max\limits_{\substack{j\in\{1,...,M_x\},\\ \beta\in\{1,2\}}} \{(u^k_{\beta_{j+1/2}})^+, -(u^k_{\beta_{j+1/2}})^+\} + \max\limits_{\substack{j\in\{1,...,M_x\},\\ \beta\in\{1,2\}}} G_\beta(p^k_{\beta_j})}, \quad \forall k \in [0, N_{it}]. \tag{4.10}$$

Proof. Assume that at a given time t^k, $\bar{n}^k_{1,j} \leq 1$ and $\bar{n}^k_{2,j} \leq 1$ for all $j \in \{1, ..., M_x\}$. The densities $\bar{n}^{k+1}_{\beta,j}$, $\beta = \{1, 2\}$, at the following time step are given by

$$\begin{aligned}
\bar{n}^{k+1}_{\beta,j} &= \bar{n}^k_{\beta,j} - \frac{\Delta t^{k+1}}{\Delta x}(F^k_{\beta,j+1/2} - F^k_{\beta,j-1/2}) + \Delta t^{k+1}\, \bar{n}^k_{\beta,j} G_1(p^k_{\beta,j}) \\
&\leq \bar{n}^k_{\beta,j} - \frac{\Delta t^{k+1}}{\Delta x}\Big[(u^k_{\beta,j+1/2})^+ \bar{n}^k_{\beta,j} + (u^k_{\beta,j+1/2})^- \bar{n}^k_{\beta,j+1} \\
&\qquad - (u^k_{\beta,j-1/2})^+ \bar{n}^k_{\beta,j-1} - (u^k_{\beta,j-1/2})^- \bar{n}^k_{\beta,j}\Big] + \Delta t^{k+1}\, \bar{n}^k_{\beta,j} G_1(p^k_{\beta,j}) \\
&\leq \Big(1 + 4\frac{\Delta t^{k+1}}{\Delta x} \max_{j\in\{1,...,M_x\}} \{(u^k_{\beta,j+1/2})^+, -(u^k_{\beta,j+1/2})^-\} + \Delta t^{k+1} \max_{j\in\{1,...,M_x\}} G_\beta(p^k_{\beta,j})\Big) \\
&\qquad \max_{j\in\{1,...,M_x\}} \bar{n}^k_{\beta,j}.
\end{aligned}$$

Adding the last inequality for the two densities we get that

$$\bar{n}_j^{k+1} \leq \Big(1 + 4\frac{\Delta t^{k+1}}{\Delta x} \max_{\substack{j\in\{1,\dots,M_x\},\\ \beta\in\{1,2\}}} \{(u^k_{\beta,j+1/2})^+, -(u^k_{\beta,j+1/2})^-\} + \Delta t^{k+1} \max_{\substack{j\in\{1,\dots,M_x\},\\ \beta\in\{1,2\}}} G_\beta(p^k_{\beta,j})\Big) \max_{\substack{j\in\{1,\dots,M_x\},\\ \beta\in\{1,2\}}} \bar{n}^k_{\beta,j}.$$

Then a sufficient condition for the total density to stay below 1 is (4.10). □

Remark 3. Eqs. (4.8) and (4.10) give conditions enabling us to choose the time step in the numerical simulations. However, in some computations we need to reduce the time step in order to avoid oscillations in the pressure when the density is close to the singular density $n = 1$. These oscillations originate from small oscillation in the densities. However despite these varations the total density still verifies the condition $0 \leq n < 1$. To enforce stability in the simulations, Δx is replaced by Δx^2 in (4.8)-(4.10) which give rise to more stringent stability constraints. This kind of condition is in fact expected for a standard parabolic CFL.

Remark 4. Similar theorems can also be proven if the second-order upwind spatial scheme from [41] is used and the forward Euler method is replaced by a higher-order SSP ODE solver since a time step in such solvers can be written as a convex combination of several forward Euler steps, see, e.g., [42, 43].

5. Conclusion

In this paper, we have presented a continuum model for two populations which avoid mixing. In addition we have introduced a numerical scheme and used it to study the behaviour of the system with different parameters. This model is a generalisation of a single population case which has been studied in the literature previously.

Through a combination of analytical and numerical arguments, this paper demonstrates that the continuum model converges to a Hele-Shaw free interface/boundary model, when an appropriate set of parameters is sent to zero (or infinity). The analytical proof is only formal and is supported by numerical simulations. In particular, we observe that the speed of the boundaries and interfaces of the continuum model for parameters taken in the asymptotic regime is the same as those computed by the Hele-Shaw model. This is verified with values of the parameters fairly far from the asymptotic regime which means that the convergence is quite fast.

Perspectives for this work are both on the analytical and numerical sides. On the analytical side, a rigorous proof of the convergence of the continuum model to the Hele-Shaw one seems within reach in the case $\alpha = 0$ and $q = 0$. On the numerical side, simulations of two-dimensional cases will be developed and applied to the modelling of tissue growth and growth termination.

Acknowledgements

The work of AC was supported in part by NSF Grant DMS-1521051, DMS-1818684 and RNMS Grant DMS-1107444 (KI-Net). SH and JPV acknowledge support from the Francis Crick Institute which receives its core funding from Cancer Research UK (FC001204), the UK Medical Research

Council (FC001204), and the Wellcome Trust (FC001204). PD acknowledges support by the Engineering and Physical Sciences Research Council (EPSRC) under grants no. EP/M006883/1, EP/N014529/1 and EP/P013651/1, by the Royal Society and the Wolfson Foundation through a Royal Society Wolfson Research Merit Award no. WM130048 and by the National Science Foundation (NSF) under grant no. RNMS11-07444 (KI-Net). PD is on leave from CNRS, Institut de Mathématiques de Toulouse, France. PD and SH would like to thank Andrea Bertozzi for stimulating discussions.

Data Statement

No new data were collected in the course of this research.

Conflict of interest

All authors declare no conflicts of interest in this paper.

AMS subject classifications

35K55; 35R35; 65M08; 92C15; 92C10

References

1. F. Otto, The geometry of dissipative evolution equations: the porous medium equation, *Comm. Part. Diff. Eq.*, **26**(2001), 101–174, URL https://doi.org/10.1081/PDE-100002243.
2. D. Kinderlehrer and N. J. Walkington, Approximation of parabolic equations using the Wasserstein metric, *ESAIM: M2AN*, **33**(1999), 837–852, URL https://doi.org/10.1051/m2an:1999166.
3. R. Jordan, D. Kinderlehrer and F. Otto, The variational formulation of the Fokker–Planck equation, *SIAM J. Math. Anal.*, **29**(1998), 1–17, URL https://doi.org/10.1137/S0036141096303359.
4. D. Drasdo and S. Höhme, A single-cell-based model of tumor growth in vitro: Monolayers and spheroids, *Phys. Biol.*, **2**(2015), 133–147.
5. J. Galle, M. Loeffler and D. Drasdo, Modeling the effect of deregulated proliferation and apoptosis on the growth dynamics of epithelial cell populations in vitro, *Biophys. J.*, **88**(2005), 62–75, URL http://www.sciencedirect.com/science/article/pii/S0006349505730873.
6. R. Araujo and D. McElwain, A history of the study of solid tumour growth: the contribution of mathematical modelling, *D.L.S. Bull. Math. Biol.*, **66**(2004), 1039.
7. D. Bresch, T. Colin, E. Grenier, et al., Computational modeling of solid tumor growth: the avascular stage, *SIAM J. Sci. Comput.*, **32**(2010), 2321–2344, URL https://doi.org/10.1137/070708895.
8. H. Byrne and M. Chaplain, Growth of necrotic tumors in the presence and absence of inhibitors, *Math. Biosci.*, **135**(1996), 187–216, URL http://www.sciencedirect.com/science/article/pii/0025556496000235.

9. P. Ciarletta, L. Foret and M. Ben Amar, The radial growth phase of malignant melanoma: multi-phase modelling, numerical simulations and linear stability analysis, *J. Royal Soc. Interface*, **8**(2011), 345–368, URL http://www.ncbi.nlm.nih.gov/pmc/articles/PMC3030817/.
10. J. Ranft, M. Basan, J. Elgeti, et al., Fluidization of tissues by cell division and apoptosis, *Proc. Natl. Acad. Sci.*, **107**(2010), 20863–20868.
11. S. Cui and J. Escher, Asymptotic behaviour of solutions of a multidimensional moving boundary problem modeling tumor growth, *Comm. Part. Diff. Eq.*, **33**(2008), 636–655, URL https://doi.org/10.1080/03605300701743848.
12. A. Friedman and B. Hu, Stability and instability of Liapunov-Schmidt and Hopf bifurcation for a free boundary problem arising in a tumor model, *Trans. Am. Math. Soc.*, **360**(2008), 5291–5342.
13. H. P. Greenspan, Models for the growth of a solid tumor by diffusion, *Stud. Appl. Math.*, **51**(1972), 317–340, URL http://dx.doi.org/10.1002/sapm1972514317.
14. J. S. Lowengrub, H. B. Frieboes, F. Jin, et al., Nonlinear modelling of cancer: bridging the gap between cells and tumours, *Nonlinearity*, **23**(2010), R1–R9, URL http://www.ncbi.nlm.nih.gov/pmc/articles/PMC2929802/.
15. D. Hilhorst, M. Mimura and R. Schätzle, Vanishing latent heat limit in a Stefan-like problem arising in biology, *Nonlinear Anal. Real*, **4**(2003), 261 – 285, URL http://www.sciencedirect.com/science/article/pii/S1468121802000093.
16. B. Perthame, F. Quirós and J. L. Vázquez, The Hele–Shaw asymptotics for mechanical models of tumor growth, *Arch. Ration. Mech. Anal.*, **212**(2014), 93–127, URL https://doi.org/10.1007/s00205-013-0704-y.
17. B. Perthame, F. Quiròs, M. Tang et al., Derivation of a Hele-Shaw type system from a cell model with active motion, *Interfaces Free Bound.*, **14**(2014), 489–508.
18. B. Perthame and N. Vauchelet, Incompressible limit of a mechanical model of tumour growth with viscosity, *Philos. Trans. R. Soc. A-Math. Phys. Eng. Sci.*, **373**(2015), 20140283, URL http://www.ncbi.nlm.nih.gov/pmc/articles/PMC4535270/.
19. H. Byrne and D. Drasdo, Individual-based and continuum models of growing cell populations: a comparison, *J. Math. Biol.*, **58**(2008), 657, URL https://doi.org/10.1007/s00285-008-0212-0.
20. J. L. Vazquez, The Porous Medium Equation: Mathematical Theory, *Oxford Mathematical Monographs*, 2007.
21. S. Hecht and N. Vauchelet, Incompressible limit of a mechanical model for tissue growth with non-overlapping constraint, *Commun. Math. Sci.*, **15**(2017), 1913–1932, URL http://www.ncbi.nlm.nih.gov/pmc/articles/PMC5669502/.
22. A. Friedman and S. Y. Huang, Asymptotic behavior of solutions of $u_t = \Delta\phi_m(u)$ as $m \to \infty$ with inconsistent initial values, *Analyse Math. Appl.*, (1988), 165–180.
23. P. Bénilan, L. Boccardo and M. Herrero, On the limit of solutions of $u_t = \Delta u_m$ as $m \to \infty$., *Interfaces Free Bound.*, **12**(1989).
24. P. Bénilan and N. Igbida, La limite de la solution de $u_t = \Delta_p u_m$ lorsque $m \to \infty$., *C. R. Acad. Sci. Paris Sier*, **321**(1995), 1323–1328.

25. C. Elliott, M. Herrero, J. King, et al., The mesa problem: diffusion patterns for $u_t = \nabla(u^m \nabla u)$ as $m \to \infty$, *IMA J. Appl. Math.*, **2**(1986), 147–154.

26. O. Gil and F. Quirós, Convergence of the porous media equation to Hele-Shaw, *Nonlinear Anal.*, **44**(2001), 1111–1131, URL http://dx.doi.org/10.1016/S0362-546X(99)00325-9.

27. A. K. Dutt, Turing pattern amplitude equation for a model glycolytic reaction-diffusion system, *J. Math. Chem.*, **48**(2010), 841–855, URL https://doi.org/10.1007/s10910-010-9699-x.

28. E. F. Keller and L. A. Segel, Initiation of slime mold aggregation viewed as an instability, *J. Theoret. Biol.*, **26**(1970), 399–415, URL http://www.sciencedirect.com/science/article/pii/0022519370900925.

29. A. J. Lotka, Contribution to the theory of periodic reactions, *J. Phys. Chem.*, **14**(1909), 271–274, URL http://dx.doi.org/10.1021/j150111a004.

30. M. Bertsch, M. E. Gurtin and L. A. P. D. Hilhorst, On interacting populations that disperse to avoid crowding: the effect of a sedentary colony, *Q. Appl. Math.*, **19**(1984), 1–12.

31. S. N. Busenberg and C. C. Travis, Epidemic models with spatial spread due to population migration, *J. Math. Biol.*, **16**(1983), 181–198, URL https://doi.org/10.1007/BF00276056.

32. M. Bertsch, R. D. Passo and M. Mimura, A free boundary problem arising in a simplified tumour growth model of contact inhibition, *Interfaces Free Bound.*, **12**(2010), 235–250.

33. M. Bertsch, D. Hilhorst, H. Izuhara, et al., A non linear parabolic-hyperbolic system for contact inhibition of cell growth, *Differ. Equ. Appl.*, **4**(2010), 137–157.

34. A. J. Sherratt and M. Chaplain, A new mathematical model for avascular tumour growth, *J. Math. Biol.*, **43**(2001), 291–312.

35. G. Galiano, S. Shmarev and J. Velasco, Existence and multiplicity of segregated solutions to a cell-growth contact inhibition problem, *Discrete Contin. Dyn. Syst.*, **96**(2015), 339–357, URL http://aimsciences.org/journals/displayArticlesnew.jsp?paperID=10564.

36. C. Elliott and Z. Songmu, On the Cahn-Hilliard equation, *Ration. Mech. Anal.*, **35**(1986), 1479–1501.

37. J. A. Carrillo, S. Fagioli, F. Santambrogio, et al., Splitting schemes and segregation in reaction cross-diffusion systems, *J. Math. Anal.*, **50**(2017),5695–5718.

38. I. Kim and A. R. Mészáros, On nonlinear cross-diffusion systems: an optimal transport approach, *Calc. Var. Partial Diff. Eq.*, **57** (2018), 79, URL https://doi.org/10.1007/s00526-018-1351-9.

39. A. Chertock, P. Degond and J. Neusser, An asymptotic-preserving method for a relaxation of the Navier–Stokes–Korteweg equations, *J. Comput. Phys.*, **335**(2017), 387 – 403, URL http://www.sciencedirect.com/science/article/pii/S0021999117300463.

40. C. Rohde, On local and non-local Navier-Stokes-Korteweg systems for liquid-vapour phase transitions, *ZAMM Z. Angew. Math. Mech*, **85**(2005), 839–857.

41. J. A. Carrillo, A. Chertock and Y. Huang, A finite-volume method for nonlinear nonlocal equations with a gradient flow structure, *Commun. Comput. Phys.*, **17**(2015), 233–258.

42. S. Gottlieb, D. Ketcheson and C. W. Shu, Strong stability preserving Runge-Kutta and multistep time discretizations, *World Scientific Publishing Co. Pte. Ltd.* (2011).

43. S. Gottlieb, C. W. Shu and E. Tadmor, Strong stability-preserving high-order time discretization methods, *SIAM Rev.*, **43**(2001), 89–112.

Appendix

A. Derivation of the continuum model

Eqs. (2.3) and (2.4) can be derived from the gradient flow associated with the free energy (2.1). Indeed the functional derivatives $\frac{\delta\mathcal{E}}{\delta n_1}$ and $\frac{\delta\mathcal{E}}{\delta n_2}$ of $\mathcal{E}$ with respect to n_1 and n_2, acting on a density increment $\tilde{n}_1(x)$ and $\tilde{n}_2(x)$ are given by

$$\frac{\delta\mathcal{E}}{\delta n_1} = p_\epsilon(n_1+n_2) + n_2 q_m(n_1 n_2) - \alpha\Delta n_1 = p_{1_{\epsilon,m}}(n_1,n_2) - \alpha\Delta n_1, \tag{A.1}$$

$$\frac{\delta\mathcal{E}}{\delta n_2} = p_\epsilon(n_1+n_2) + n_1 q_m(n_1 n_2) - \alpha\Delta n_2 = p_{2_{\epsilon,m}}(n_1,n_2) - \alpha\Delta n_2. \tag{A.2}$$

Indeed, the computation for the first derivative is given by

$$\begin{aligned}
< \frac{\delta\mathcal{E}}{\delta n_1}, \tilde{n}_1 > \;&:=\; \int_{\mathbb{R}^d} \frac{\delta\mathcal{E}}{\delta n_1}(n_1,n_2)\,\tilde{n}_1 dx \\
&=\; \lim_{h\to 0}\frac{1}{h}\Big(\mathcal{E}(n_1+h\tilde{n}_1,n_2) - \mathcal{E}(n_1,n_2)\Big) \\
&=\; \lim_{h\to 0}\frac{1}{h}\int_{\mathbb{R}^d}\Big(P_\epsilon(n_1+h\tilde{n}_1+n_2)(x) - P_\epsilon(n_1+n_2)(x)\Big)\,dx \\
&\quad + \lim_{h\to 0}\frac{1}{h}\int_{\mathbb{R}^d}\Big(Q_m((n_1+h\tilde{n}_1)n_2)(x) - Q_m(n_1 n_2)(x)\Big)\,dx \\
&\quad + \lim_{h\to 0}\frac{\alpha}{2h}\int_{\mathbb{R}^d}\Big(|\nabla(n_1+h\tilde{n}_1)|^2 - |\nabla n_1|^2\Big)\,dx \\
&=\; \int_{\mathbb{R}^d}\Big(\frac{\partial P_\epsilon}{\partial n_1}(n_1+n_2) + \frac{\partial Q_m}{\partial n_1}(n_1 n_2) + \alpha\nabla n_1\nabla\tilde{n}_1\Big)\,\tilde{n}_1 dx \\
&=\; \int_{\mathbb{R}^d}\Big(p_\epsilon(n_1+n_2) + n_2\, q_m(n_1 n_2) - \alpha\Delta n_1\Big)\,\tilde{n}_1 dx.
\end{aligned}$$

The expression of $\frac{\delta\mathcal{E}}{\delta n_2}$ follows from a similar computation. Therefore the gradient flow associated to the free energy (2.1) according to the Wasserstein metric can be written as follows [1],

$$\partial_t n_1 - \nabla\cdot(n_1\nabla\frac{\delta\mathcal{E}}{\delta n_1}(n_1,n_2)) = 0, \tag{A.3}$$

$$\partial_t n_2 - \nabla\cdot(n_2\nabla\frac{\delta\mathcal{E}}{\delta n_2}(n_1,n_2)) = 0. \tag{A.4}$$

The metric used here is not the traditional distance on $L^2(\mathbb{R}^d)$, but the Wasserstein distance. This distance is defined on the set of probability distributions on $\mathbb{R}^d$. It is used in a wide variety of physically

meaningful equations like the porous medium equation or degenerate parabolic equations [2, 3, 1]. We recover Eqs. (2.3) and (2.4) of the SPM by adding growth terms G_1 and G_2 to (A.3) and (A.4).

It is worth noting that the free energy decreases along the trajectories of the equation in the absence of growth terms. Indeed, using the Green formula and the Eqs. (A.3) and (A.4), we have

$$\begin{aligned}
\partial_t \mathcal{E}(n_1, n_2) &= \int_{\mathbb{R}^d} \Big(\frac{\delta \mathcal{E}}{\delta n_1}(n_1(x,t), n_2(x,t))\, \partial_t n_1(x,t) \\
&\quad + \frac{\delta \mathcal{E}}{\delta n_2}(n_1(x,t), n_2(x,t))\, \partial_t n_2(x,t)\Big)\, dx \\
&= \int_{\mathbb{R}^d} \Big(\frac{\delta \mathcal{E}}{\delta n_1}(n_1(x,t), n_2(x,t)) \nabla \cdot (n_1(x,t) \nabla \frac{\delta \mathcal{E}}{\delta n_1}(n_1(x,t), n_2(x,t))) \\
&\quad + \frac{\delta \mathcal{E}}{\delta n_2}(n_1(x,t), n_2(x,t)) \nabla \cdot (n_2(x,t) \nabla \frac{\delta \mathcal{E}}{\delta n_2}(n_1(x,t), n_2(x,t)))\Big)\, dx \\
&= -\int_{\mathbb{R}^d} n_1(x,t) \Big|\nabla \frac{\delta \mathcal{E}}{\delta n_1}(n_1(x,t), n_2(x,t))\Big|^2\, dx \\
&\quad - \int_{\mathbb{R}^d} n_2(x,t) \Big|\nabla \frac{\delta \mathcal{E}}{\delta n_2}(n_1(x,t), n_2(x,t))\Big|^2\, dx \le 0.
\end{aligned} \tag{A.5}$$

Therefore, when the growth rates are set to 0, the model evolves in a way that minimize the free energy. This free energy depends on three terms, representing the levels of volume exclusion, segregation and cohesion. Therefore the model seeks to minimize the pressures, which means moving away from situations where the volume exclusion or the segregation constraints are violated.